NASA Contractor Report 4404

Lunar Dust Transport and Potential Interactions With Power System Components

Cynthia M. Katzan and Jonathan L. Edwards

CONTRACT NAS3-25266
NOVEMBER 1991

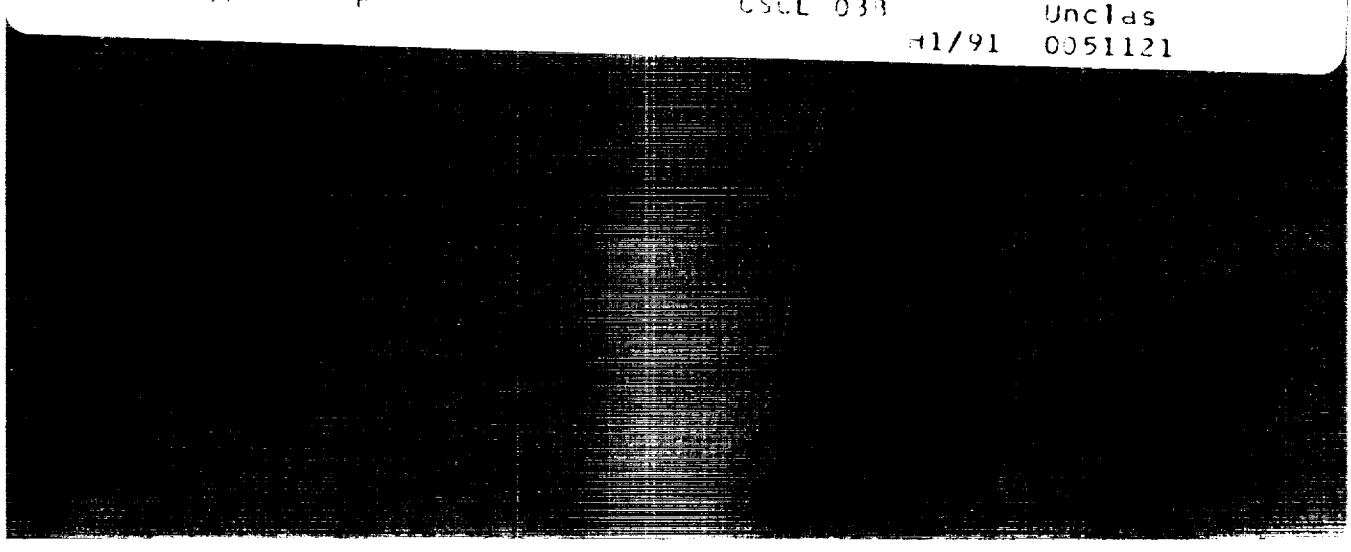

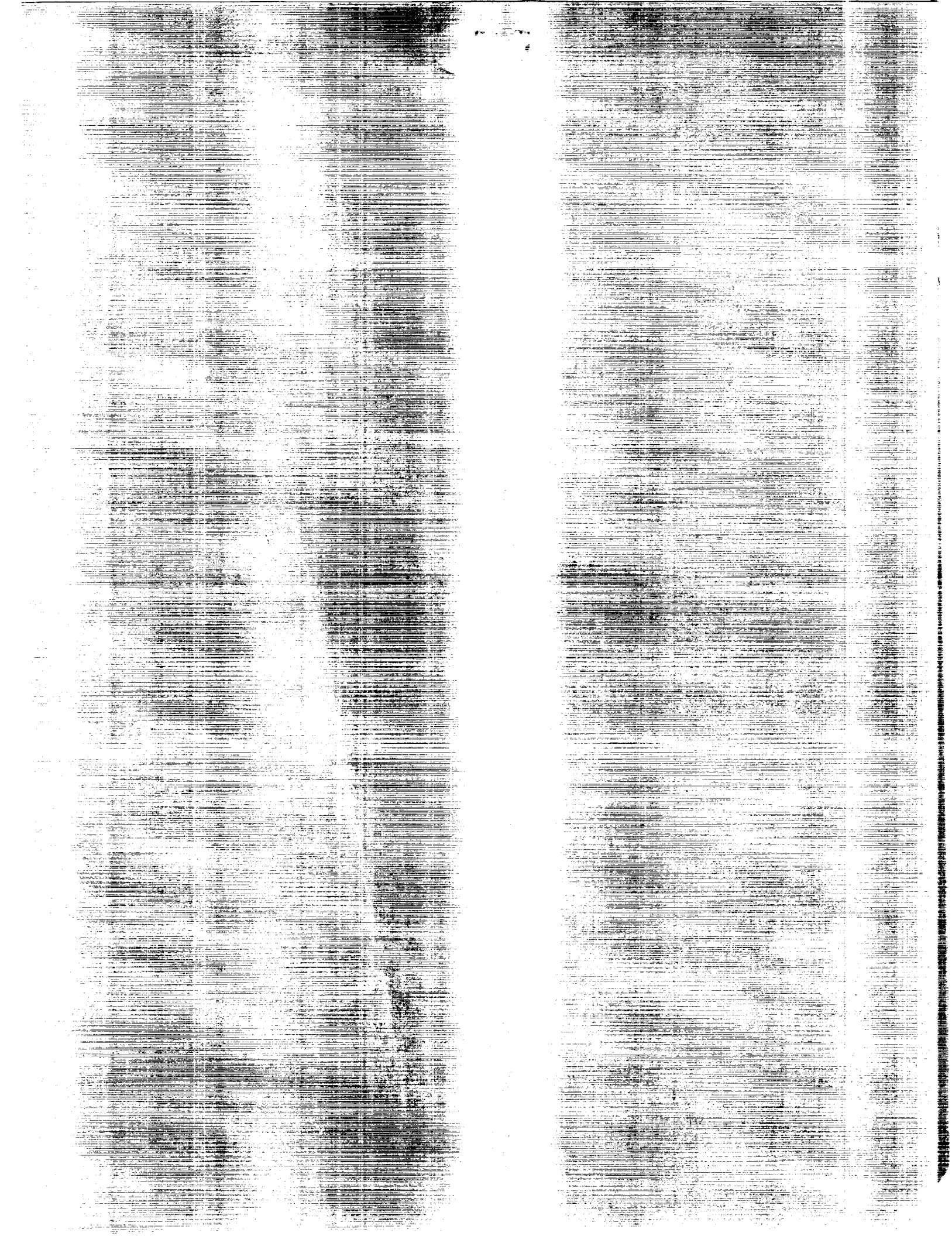

NASA Contractor Report 4404

Lunar Dust Transport and Potential Interactions With Power System Components

Cynthia M. Katzan
Sverdrup Technology, Inc.
Lewis Research Center Group
Brook Park, Ohio

Jonathan L. Edwards
Marshall University
Huntington, West Virginia

Prepared for
Lewis Research Center
under Contract NAS3-25266

National Aeronautics and
Space Administration

Office of Management

Scientific and Technical
Information Program

1991

Summary

The lunar surface is covered by a thick blanket of fine dust. This dust may be readily suspended from the surface and transported by a variety of mechanisms. As a consequence, lunar dust can accumulate on sensitive power components, such as photovoltaic arrays and radiator surfaces, reducing their performance. In addition to natural mechanisms, human activities on the Moon will disturb significant amounts of lunar dust. Of all the mechanisms identified, the most serious is rocket launch and landing. The return of components from the Surveyor III provided a rare opportunity to observe the effects of the nearby landing of the Apollo 12 lunar module. The evidence proved that significant dust accumulation occurred on the Surveyor at a distance of 155 m. From available information on particle suspension and transport mechanisms, a series of models was developed to predict dust accumulation as a function of distance from the lunar module. The accumulation distribution was extrapolated to a future lunar lander scenario. These models indicate that accumulation is expected to be substantial even as far as 2 km from the landing site. Estimates of the performance penalties associated with lunar dust coverage on radiators and photovoltaic arrays are presented. Because of the lunar dust adhesive and cohesive properties, the most practical dust defensive strategy appears to be the protection of sensitive components from the arrival of lunar dust by location, orientation, or barriers.

Introduction

The harsh lunar environment will provide many challenges to the designers of a manned lunar base. Such challenges include identifying and compensating for the biological effects of low gravity, preventing ultraviolet (UV) degradation of materials, preparing for temperature extremes, and protecting against solar flares, meteoroid impact, and ionizing radiation. However, despite their potential impact, relatively little attention has been given to the consequences of operating a manned lunar base in a dusty environment.

After only hours on the lunar surface, the Apollo astronauts observed that lunar dust was the source of certain aggravating operational problems. They reported that it had the capacity to get everywhere. The O-ring seals of their suit gloves and helmets became "bogged down with dust," and dust interfered with their mechanical pulleys and zippers (Apollo 12 Technical Crew Debriefings, 1969). During the rover operations, cameras became obscured, and rover batteries and radiators had to be brushed clean at every stop (Morris, 1973). A color contrast chart was dropped and rendered useless, because lunar dust simply does not wipe off readily. For the Apollo Program, lunar dust problems were troublesome but tolerable, and did not severely jeopardize mission objectives.

However, to assure successful 30-yr mission capabilities for a manned lunar base, the effects of lunar dust transport must be given serious consideration during base design and operations planning. Of the many dust-sensitive base components, lunar dust accumulation may have the greatest impact on critical power system surfaces such as photovoltaic arrays and radiator surfaces.

Photovoltaic and radiator surfaces are of particular interest because they are vulnerable to the accumulation of lunar dust, and they are critical in furnishing required power. The two most likely candidates for a permanent lunar base power source are photovoltaic array/regenerative fuel cell combinations and nuclear reactors. Thus, the potential interference of lunar dust with the performance of these components will pose significant implications on the lunar base configuration.

Even in the event that alternate power systems are developed for the lunar base, the susceptibility of photovoltaic arrays and radiators to dust accumulation will still be an important issue. Temporary solar arrays may be deployed to power operations until construction of a permanent power system is complete, and radiators will have a significant role in any heat rejection associated with the conditioning, distribution, and management of power. The effects of dust on other sensitive surfaces, such as windows, lenses, reflectors, and antennas, may also be derived from an understanding of the effects of lunar dust accumulation on power system surfaces.

After a brief description of lunar soil, this report presents several mechanisms by which lunar particles may be suspended from the Moon's surface. Of these, launch and landing are expected to be the greatest threat to power system surfaces. As such, they are the primary focus of this report. The available evidence for dust suspension by spacecraft landing is presented, and particle trajectories and accumulations are estimated. Finally, the dust-related penalties in power component performance are projected.

Properties of Lunar Dust

The surface gravitation on the Moon is about one-sixth that on Earth—roughly 1.63 m/s^2. This is too weak to retain an

atmosphere, except for trace He, H_2, Ne, and Ar, and even smaller amounts of CO_2 and H_2O. The atmospheric pressure at the lunar surface was observed to be less than 8×10^{-9} torr during the Apollo 12 mission (West, Wright, and Euler, 1977). Some of these gases are trapped in the soil during the cold lunar night (100 K), and escape as the surface heats up from the sun. At the hottest point of the lunar day, when the surface temperatures peak at 400 K, the "atmospheric" concentration of He is only 2×10^3 atoms/cm^3 (Taylor, 1975). The trace gases, therefore, offer no protection against micrometeoroids, solar wind, or cosmic and solar radiation.

The lunar "regolith" is the blanket of soil and rocks 3 to 20 m thick that covers the lunar surface. Its components range in size from very fine dust to enormous "blocks" that have no observable organization into layers. Often solitary rocks dot an expanse of fine soil. Approximately 70 wt % of the regolith is composed of silty soil of particles less than 1 mm in diameter (J. Graf, 1989, NASA Johnson Space Center, Houston, TX, personal communication); 50 wt % of the soil is finer than 50 μm (see fig. 1, taken from Smith and West, 1983).

The size, morphology, and compositional mixing of the regolith material are the result of complex natural comminution (destruction) and agglutination (construction) processes occurring over geologic time. These include meteoroid impact, thermal cycling, creep, and solar wind erosion.

The regolith is composed of several minerals that are also found on Earth. Among the main minerals are familiar basaltic components: plagioclases (mostly anorthite), olivine, and pyroxenes. Other minerals, such as ilmenite, cristobalite, and apatite, and natural metals, like Fe and Ni, are also observed. In addition, as much as 20 wt % of the soil may be glassy material, ranging in color from orange to green to black (Morris et al., 1983). The relative amounts of these minerals vary somewhat between the two main topographical regions: the maria, or "seas," and the highland regions.[1] It is thought that roughly 3.5 billion years ago fresh basalt flows covered the maria, causing the soil there to be richer in Fe, Ti, and Mg—mostly in the form of ilmenite ($FeTiO_3$), olivine ($(Mg,Fe)_2SiO_4$), and other minerals. In contrast, the highlands may contain as much as 60 wt % anorthite ($CaAl_2Si_2O_8$), whereas the maria may only contain 35 wt % (Inculet and Criswell, 1979). The chemical compositions of typical soils from the highlands and maria are compared in table I. Because compositional variations are very localized, it appears that there is little lateral mixing between regions (Papike, Simon, and Laue, 1982).

The overall particle size range of lunar soil is shown in figure 1. From this it can be seen that mare soils (Apollo 11 and 12), highland soils (Apollo 14), and material from the mare-highland interface (Apollo 15) do not differ greatly in overall particle size. However, some differences in composition with particle size have been discussed by Papike, Simon, and Laue (1972). Particles smaller than 10 μm tend to be enriched in Al_2O_3, most likely because of the susceptibility of feldspars (anorthite) to comminution relative to olivine and the pyroxenes. For the same reason, this size fraction is also enriched in CaO, Na_2O, K_2O, Th, and light rare earth elements, while being depleted in Sc, MgO, MnO, and FeO. From 10 to 90 μm, the Al_2O_3 content decreases, but from 90 to 1000 μm, the Al_2O_3 content again increases. This increase is attributed to the abundance of agglutinates (welded particle clumps), which are composed of very fine particles. The concentrations of Sc, MgO, MnO, and FeO increase from 10 to 90 μm and decrease from 90 to 1000 μm, accordingly.

Because of the unusual erosion mechanisms on the Moon, the particle morphology is unlike that which is usually found on Earth. Lunar particles range in shape from spherical glass beads to highly vesicular[2] agglutinates, largely because of the

TABLE I.—TYPICAL LUNAR SOIL COMPOSITION

[Data taken from Morris et al., 1983.]

Major compositional elements	Maria,[a] wt %	Highlands,[b] wt %
SiO_2	40.09	44.2
TiO_2	9.23	.26
Al_2O_3	10.70	29.4
Cr_2O_3	.49	-----
FeO	17.85	2.96
MnO	.24	.6
MgO	9.92	16.30
CaO	10.59	.73
Na_2O	.36	.11
K_2O	.08	-----

[a]Soil 71060, Apollo 17.
[b]Soil 67710, Apollo 16.

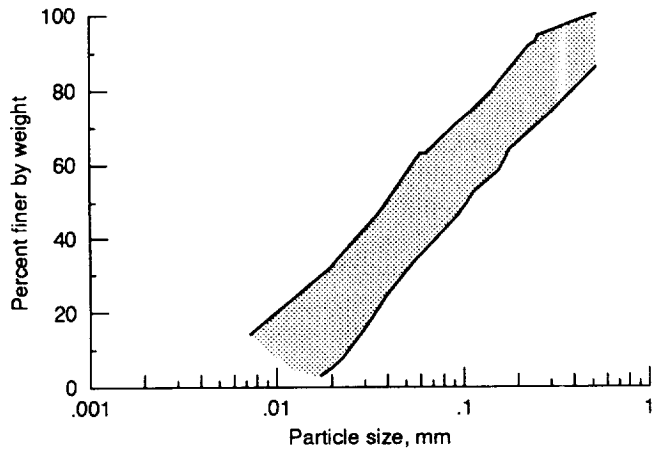

Figure 1.—Grain size distribution for lunar soil. Samples from Apollo 11, 12, 14, and 15 all fall within this band (Smith and West, 1983).

[1]The near side of the Moon has both maria and highlands. The far side is almost exclusively highlands.
[2]"Vesicular" refers to a morphology much like lava rock, characterized by many pockets or cavities.

effects of hypervelocity meteoroid impacts. These impacts result in particle comminution by crushing and vaporizing particles in the target area. Conversely, hypervelocity impacts are also responsible for vapor- and melt-welding particles together to form agglutinates.

Agglutinates are a very important component of the lunar regolith. As much as 50 or 60 percent of the soil is agglutinated (D.S. McKay, 1989, NASA Johnson Space Center, Houston, TX, personal communication), and consequently three or four minerals are usually present in every particle. In addition, agglutinates tend to have tortuous morphologies depending on the size of their substituent grains. The result is an overall soil equivalent surface area ratio of 60 (the average particle has 60 times the surface area of a sphere of the same mass) (Carrier, 1990). This high surface area affects such properties as cohesion, compressibility, and shear strength.

Soils that have the highest fraction of agglutinates are termed "mature." Maturity is quantified by the ratio of Fe metal to Fe oxides (material with Fe:FeO < 30 is classified as immature, 30 < Fe:FeO < 60 as submature, and Fe:FeO > 60 as mature). Because a mature soil has been more completely "worked" by natural forces, its agglutinate chemical composition is closer to the bulk composition than is true for immature soils. Also, in mature soils there is said to be a balance between comminution and agglutination processes so that the particle size distribution is at a steady state (McKay, Fruland, and Heiken, 1974).

Through various lunar soil mechanics experiments, it was learned that lunar soil exhibits strong cohesive forces. The main forces between lunar particles are van der Waals and electrostatic interactions. Generally speaking, van der Waals forces include attractions associated with permanent dipoles, dipoles induced by an external polarity, and dispersion forces (often called London-van der Waals dispersion) which arise from instantaneous dipoles between neighboring atoms or groups of atoms. Van der Waals forces generally predominate over other forces for very small particles, such as those which make up the bulk of the regolith.

However, electrostatic forces are also important because the lunar soil is electrically insulating. The electrical conductivity at 27 °C is in the neighborhood of 10^{-13} to 10^{-16} $\Omega^{-1}m^{-1}$ from dc measurements (Strangway, 1969). (As a reference of comparison, for polytetrafluoroethylene this value is roughly 10^{-16} $\Omega^{-1}m^{-1}$.) Electrostatic forces are generally broken down into classical coulombic effects and contact potential. Contact potential is related to the difference in work function between two materials in contact, which can induce electrons to move from the higher work function material to the other. For lunar soil, London-van der Waals dispersion forces and contact potential are the dominating forces. The vacuum environment of the Moon tends to enhance the magnitudes of both these forces, because gas is not available to compensate charges. As a result, lunar particle cohesion has been estimated to be roughly 0.035 to 0.05 N/cm^2 from lunar surface experiments (Jaffe et al., 1969). As an illustration, trenches carved 17.5 cm deep into the lunar surface retained vertical walls without sliding (Scott, Robertson, and Clary, 1967). On Earth, this degree of cohesion is often simulated with wet sand.

The adhesion of lunar particles to a surface is driven by the same types of forces. During the Apollo missions, adhesive forces were observed to vary somewhat with the surface type, from roughly 0.01 to 0.1 N/cm^2 for metallic surfaces to about 0.1 N/cm^2 for painted surfaces. Lunar particle adhesion to teflon is somewhere in between (Nickel and Carroll, 1972). According to the Apollo astronauts, lunar dust clung tenaciously to everything it contacted, and removal efforts were futile.

Natural Mechanisms for Lunar Dust Transport

Because of the lack of atmosphere, particle suspension and transport on the Moon do not occur by familiar terrestrial mechanisms. Two natural mechanisms have been identified that are unique to the lunar environment and which may potentially contribute to lunar dust accumulation on power surfaces.

The first is meteoroid impact into the lunar surface. Zook et al. (1984, 1985) proposed that many lunar particles are sprayed out as "secondary ejecta" with each primary meteoroid impact. They correlated an anomalously high incidence of small lunar impact craters (especially smaller than 7 μm) with the showers of secondary ejecta. The number of these secondary ejecta depends on the size and velocity of the incoming meteoroid, but a single typical hypervelocity meteoroid impacting at 20 km/s may eject 100 to 1000 times its mass in secondary particles, depending on its angle (H.A. Zook, 1989, NASA Johnson Space Center, Houston, TX, personal communication). The estimated cumulative primary meteoroid flux is shown in figure 2, and the associated secondary flux is shown in figure 3 (data taken from West, Wright, and Euler, 1977). According to these estimates, for

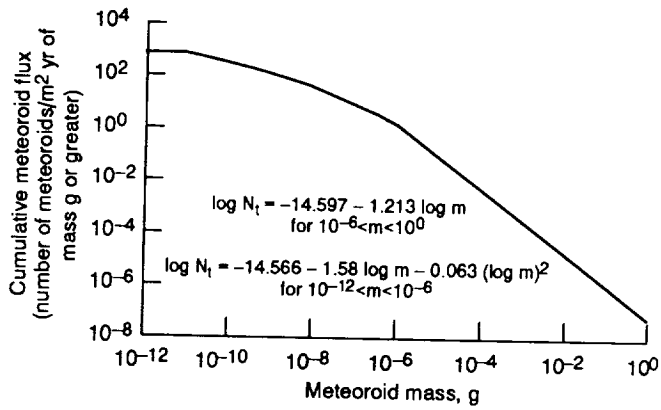

Figure 2.—Cumulative meteoroid flux at the lunar surface. (Equations taken from West, Wright, and Euler, 1977.)

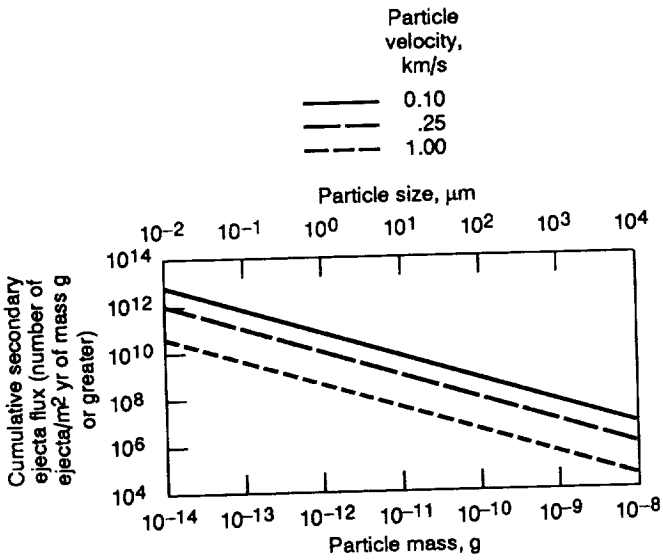

Figure 3.—Lunar secondary ejecta distribution. (Data taken from West, Wright, and Euler, 1977.)

example, every square meter of the Moon's surface is impacted by an average of 95 primary meteoroids, 1 ng or bigger, each year. More than 30 million lunar secondary ejecta that are 1 ng or bigger are suspended with a velocity of 1.0 km/s from these primary impacts. (The lunar escape velocity is 2.3735 km/s.) From figures 2 and 3 it is possible to extrapolate that roughly 10^{-7} and 10^{-1} g/m^2-yr of material is transported through primary and secondary ejecta, respectively. Though relatively infrequent, the effects of secondary, and therefore also primary, impacts could contribute to the accumulation of dust on surfaces over the 30-yr lifetime of a lunar base.

The second natural mechanism for suspending lunar dust is an electrostatic effect at the Moon's sunset terminator (the boundary between the lit and unlit sides of the Moon). This effect has been proposed by Criswell and his colleagues as an explanation for a phenomenon known as "horizon glow": a thin, bright streak traces the horizon in photographs of the lunar sunset. This streak is attributed to the diffraction of light off a low cloud of lunar particles. According to Criswell (1973) and Pelizzari and Criswell (1978), soil particles on the sunlit side near the terminator become positively charged because of the photoelectric effect from solar UV radiation. These charged particles hop up and over to the dark side of the terminator, where some of the photoelectrons have accumulated. The result is a "churning" of soil as the terminator progresses across the Moon, with particles hopping 3 to 30 cm from the lunar surface. By this theory, a projected 300 g/m^2 of lunar soil is electrostatically levitated each year. This rate of transport was estimated to be roughly 6×10^7 greater than the rate of primary meteoroids, and 2×10^5 times greater than the rate of secondary micrometeoroids (Rennilson and Criswell, 1974), consistent with the accumulations derived from figures 2 and 3.[3]

The effects of these natural dust-suspending mechanisms may be potentially serious to power components on a lunar base. They are eternal processes and geographically widespread; their sources fall outside human control. Moreover, additional natural mechanisms may exist that have not yet been observed, but which will also contribute to dust suspension. However, compared with those mechanisms associated with human activity on the lunar surface, the effects of natural dust-suspending mechanisms appear decidedly minor.

Dust Suspension Caused by Human Activity

Four areas of human activity have been identified which are potentially threatening to dust-sensitive power surfaces. These activities are predicted to locally suspend substantially greater amounts of dust than natural mechanisms. Although it is certain that these activities will be standard to lunar base operation, their extent and frequency are subject to base objectives and design. The dust transported by human activity will be discussed in order of increasing severity.

Walking

The first human-related mechanism is simply walking on the lunar surface. The Apollo astronauts indicated that this was not accomplished in the same manner as on Earth—instead, in low gravity and with large protective boots, walking is rather a side-to-side wobbling with occasional shuffling. This is inevitably accompanied by the kicking of the fine lunar material, either forward or to the side. Because there is no atmosphere, the majority of the particles move in fan-like sprays, spreading out from the boot at an angle corresponding to the kick direction. This effect can easily be seen on video footage of the astronauts' lunar walks. In fact, each astronaut acquired substantial coverage on his leggings from the dust sprays of the other astronaut (see fig. 4). Assuming Earthlike mobility and a normal pace of 4 mph (1.8 m/s), the boot velocity in a normal walking kick might be on the order of 3.6 m/s. Space suit design may evolve to match this degree of mobility, and therefore the resultant particle sprays could reach comparable speeds for each hobble

[3] The electrostatic levitation of dust has also been suggested by the Lunar Ejecta and Meteorite (LEAM) experiment deployed by Apollo 17. A conspicuous increase in the particle event rate occurs with each lunation, lasting roughly 70 hr. Although the actual electric potentials across the terminator are still unknown, preliminary laboratory experiments have confirmed that such levitation is possible with charged gold particles (Rhee, Berg, and Worf, 1977).

Alternative explanations of this phenomenon are few. One that may be worthy of mention is the reflection off raised landscape features which are located on the "dark side" of the terminator but which still receive the low angle light from the setting sun because of their height (Allen, 1969).

ORIGINAL PAGE
BLACK AND WHITE PHOTOGRAPH

Figure 4.—Photograph of Apollo astronaut Conrad inspecting the Surveyor III spacecraft. The lunar module is visible in the background. The astronaut's leggings and gloves are covered with lunar dust from activities on the Moon's surface (AS12-48-7133).

and shuffle. The disturbed particles will experience pure Newtonian motion, independent of size or shape. The maximum range will be achieved by those particles kicked at 45°, according to simple projectile mechanics:

$$\text{range} = \frac{v_0^2 \sin 2\phi}{g} \tag{1}$$

where v_0 is the initial particle velocity, ϕ is the ejection angle with respect to the surface, and g, the lunar surface gravitation constant, is 1.63 m/s^2. (A complete symbols list is provided in appendix A.) The maximum particle height is determined when the initial motion is entirely vertical (that is, when the vertical component of the initial velocity, v_{0y}, equals v_0), and it is solved when vertical velocity, $v_y(t)$, is zero:

$$v_y(t) = v_{0y} - gt = 0 \qquad t = \frac{v_{0y}}{g} = 2.2 \text{ s} \tag{2}$$

where t indicates time in seconds;

$$y = v_{0y}t - \frac{gt^2}{2} = 4 \text{ m} \tag{3}$$

This range and height are considerably greater than observed on Earth, since there are not enough gas molecules to moderate lunar particle trajectories. Perhaps the most important concern about walking is that it will be a close-range source of lunar dust for sensitive power components. The construction, maintenance, and repair of power facilities will all require some degree of direct astronaut contact. Consequently, the dust accumulation may be directly related to the self-sufficiency of the power facilities.

Rover Operation

The lunar roving vehicles are likely to disturb significantly more lunar dust than walking. In low-gravity experiments, the amount of dust produced by the slow turning of a rover wheel in simulated lunar dust was extensive (Mullins, 1971—also see the associated videotapes in the Washington National Records Center, roll # 0-2890-91, 92, 93, accession # 255-80-0901, location 03-07-04-2-1, box 11, cans 103-105, 108, 109). From these studies, it was determined that dust is not just cast out the back of the wheel, but also gets carried over the wheel and "poured" off the front, sprayed out the side, tumbled through the mesh wheel, and bulldozed before the wheel. When there is no slip between the wheel and soil, the greatest velocity is attained by those particles hurled off the top of the wheel. Their net velocity is the summation of the velocity vector associated with the wheel's rotation v_{rot} and the translational velocity vector v_{trans}, which each have the magnitude and direction of v_{rover}. The Apollo lunar rovers were designed to travel at a maximum of 3.56 m/s (8 mph) (Baker, 1971) so these particles have speeds of up to 7.12 m/s in the forward direction. If for some reason such a particle were to have an elastic collision with another rover component at an oblique impact angle of 45°, it can be shown that the particle's direction would be changed to 45° from the horizontal, with no loss in magnitude. The 45° trajectory will yield the maximum horizontal distance, and therefore the particle could travel as far as 31 m (103 ft) from the wheel's initial location.

By far, however, the bulk of the disturbed dust is ejected in the form of a characteristic "rooster tail." In this discussion a fenderless wheel will be assumed in order to demonstrate the potential for dust transport, and thus the importance of careful fender design. Through simple laws of projectile motion, and assuming no slip, it can be shown that the particles that make up this plume are actually moving forward with the rover, and not "backward." In other words, the sum of the rotational and translational velocity components always has a positive $\hat{x}$ component:

$$\begin{aligned} v_{total} &= \left(v_{rot} = v_{trans}\right)\hat{x} + \left(v_{rot}\right)\hat{y} \\ &= \left(v_{rover}\cos\Theta + v_{rover}\right)\hat{x} + \left(v_{rover}\ sin\,\Theta\right)\hat{y} \end{aligned} \tag{4}$$

For these calculations, the positive $\hat{x}$ direction is the direction of the rover's motion, and Θ defines the point on the wheel at the instant when the particle is released.[4] The distance traveled by an ejected particle is a function of Θ:

$$x = 2\left(v_{rover}\right)^2 \frac{(1 - cos\ \Theta)(\sin\Theta)}{g} \tag{5}$$

This distance is measured from the wheel's instantaneous point of contact with the lunar surface when the particle was ejected. The vertical and horizontal positions of the particle at the instant of ejection relative to this origin are neglected. Consequently, dust particles ejected at angles beyond 180° are not projected.

Figure 5 shows particle distance versus wheel angle Θ at ejection. The maximum distance is attained by particles ejected when Θ equals 120°. These particles actually travel 20.4 m (67 ft), landing ahead of the rover. Such particles could become a threat when a rover drives toward a solar array or radiator structure. The accumulation of dust at different distances is difficult to establish. However, assuming particles ejected at all Θ with equal frequency (a gross simplification), it is reasonable to expect the accumulation distribution to be inversely proportional to the derivative, $dx/d\Theta$, of

[4]Note that Θ does not necessarily correspond to the ejection angle. The ejection angle results from the sum of the vectors associated with rotational and translational motion.

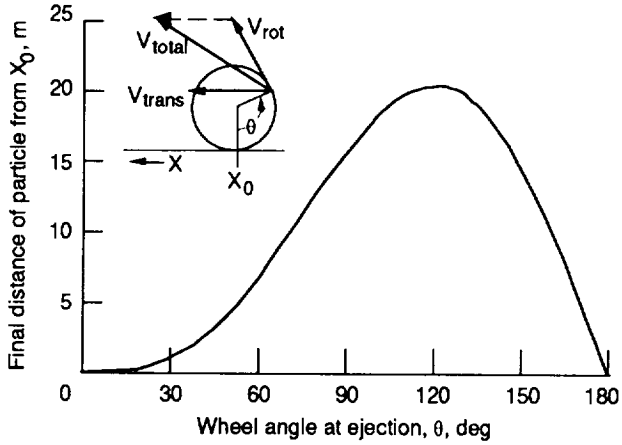

Figure 5.—Predicted distance traveled by particles ejected at various angles by a fenderless lunar roving vehicle moving at 3.56 m/s.

equation (5). That is, the greater the change in distance between falling particles for a given change in ejection angle, the lower the accumulation at that distance. Thus the dust accumulation distribution $N(\Theta)$, in mass/area, is given by

$$N(\Theta) \propto \left(\frac{dx}{d\Theta}\right)^{-1} \tag{6}$$

The distribution $N(\Theta)$ has been converted to $N(x)$ and plotted in figure 6. As can be seen, a large number of particles land both in the vicinity of the wheel, as well as at a distance of 20.4 m ahead of the wheel's original location. Physically, this occurs because at $\Theta = 0°$ dust particles have no velocity and because at $\Theta = 120°$ (corresponding to dust projected 20.4 m) there is great insensitivity to ejection angle. With a more realistic ejection distribution, the dominance of these particles in the accumulation distribution will be tempered. Nevertheless,

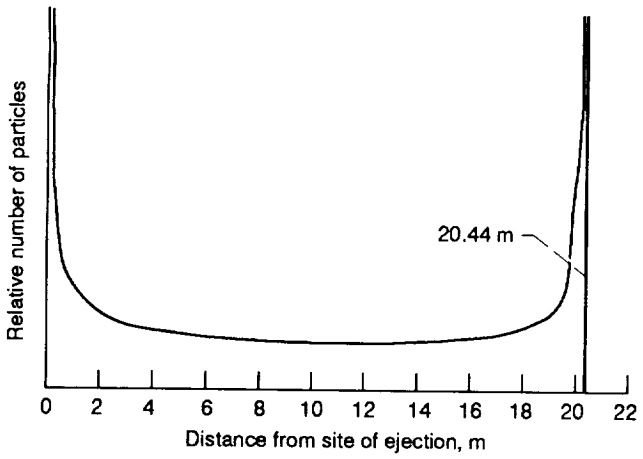

Figure 6.—Predicted particle accumulation distribution as a function of distance from the site of ejection from a fenderless lunar rover wheel moving at 3.56 m/s. A uniform ejection distribution has been assumed. At most, particles travel 20.4 m in the forward direction when there is no slip.

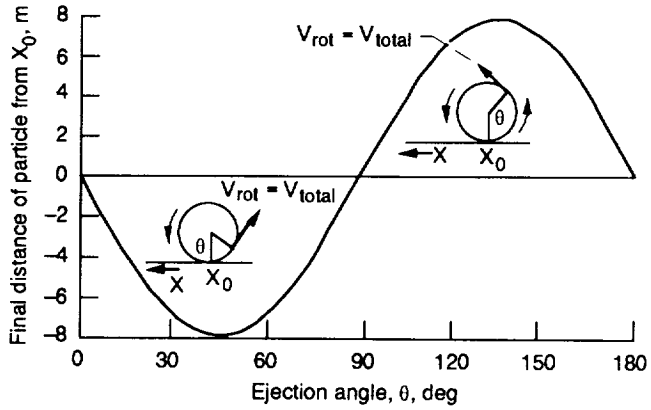

Figure 7.—Predicted distance traveled by particles ejected from a fenderless rover at various wheel angles, assuming 100-percent slip on the lunar surface. In this example, the wheel rotational velocity has a magnitude v_{rot} = 3.56 m/s.

this illustrates the extreme importance of proper fender design, and may impact the selection of solar or nuclear power for surface vehicles.

In Apollo video footage of a "test drive" of the rover on the lunar surface, the dust sprays were particularly dramatic during sharp turns and bounding on rough terrain. These dramatic sprays occur when there is momentary slip between the wheel and surface. Under such conditions, the rotational component of motion may make up as much as 100 percent of the motion transferred from the wheel to the particle. In the case of 100 percent slip (100 percent rotation and no translational motion), particles leaving at a wheel angle between 0° and 90° do indeed travel backward, and those leaving at Θ greater than 90° move in the forward direction. Distance is maximized when Θ is 45° or 135° (see fig. 7). If it is assumed that the magnitude of the rotational velocity vector is on the order of 3.56 m/s, particles can travel up to 8 m (26 ft), backward or forward. It is more likely that during "free-wheeling" the rotational velocity is considerably greater. In a manner similar to that discussed earlier, the accumulation distribution is related to the inverse of the change in distance with ejection angle (see fig. 8). This profile is dominated by those particles ejected at 45° and 135° when a uniform ejection distribution is employed. However, the accumulation distribution is expected to reflect a greater number of short-distance trajectories when the ejection distribution is skewed to smaller angles, where fender design is critical but difficult.

The ejection of dust by moving vehicles appears to be inevitable, because of the coarse terrain and the overwhelming presence of dust. The use of surface vehicles in facility maintenance and general base transportation may often bring this source of suspended dust dangerously close to power components. The extent to which the next generation of lunar rovers disturb dust depends in part on their design, but perhaps even more critically on their role as an integral part of base operation.

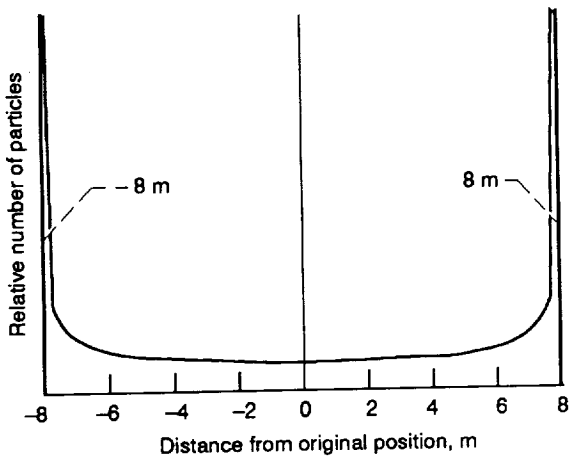

Figure 8.—Predicted particle accumulation distribution as a function of distance from the site of ejection from a fenderless lunar rover wheel spinning at 3.56 m/s with 100-percent slip. A uniform ejection distribution has been assumed. At most, particles travel 8 m in the positive and negative x direction.

Mining and Construction

Mining and construction will also be important contributors to dust suspension on the Moon. Their effects may be the most difficult to assess for several reasons: (1) The actual resources to be mined and the methods for doing so have not been established; (2) the building types proposed thus far range from "habitrail" units transported from Earth to buried inflated bubble chambers covered with lunar sandbags; and finally, (3) many subactivities are involved in both mining and construction. However, it can be assumed that large, powerful, but slow-moving, vehicles will be employed with the versatility to accomplish several different tasks. These vehicles will probably not attain the speeds of the rovers or have great agility, so particle speeds are not expected to exceed 7.12 m/s. However, their main functions will be mass manipulation of lunar soil, and thus dust disturbance is guaranteed. Between mining and construction, there will likely be much "earthmoving," digging, dumping, and transporting of soil. Mining may be reserved for remote areas, but the refining and processing may need to be performed near sources of power, and enormous loads of lunar material will need to be transported in and out of the vicinity of power facilities. Construction may be a continual process as the lunar base evolves. It will include clearing obstructions in new areas and constructing habitats, laboratories, processing plants, storage warehouses, and the power facilities themselves. Multibody collisions may enable some fractions of small particles to reach high velocities, and therefore also great distances, unlike on Earth where atmospheric drag quickly slows down such fast, small particles. Dusty as a terrestrial construction site is, a lunar construction site or mining area will be considerably worse because of the unchecked travel of particles under vacuum and the weaker surface gravity.

Spacecraft Landing

Perhaps the single most significant human activity that suspends lunar dust is the ascent and descent of space vehicles at the lunar surface. A recent study estimated that approximately 48 missions from Earth (manned and unmanned) will be necessary to establish a lunar base over 6 yr (Lunar Base Launch and Landing Facility Conceptual Design, 1988). In addition, planners forecast that a trip will be required at least every 6 mo to satisfy the maintenance needs of base facilities and personnel. These trips could sum to more than 108 landings and 108 launches during the 30-yr lifetime of a lunar base. According to the observations of the Apollo astronauts (discussed next), the amount of dust produced on landing is enormous. The possible dust problems associated with spacecraft launch and landing on the lunar surface are thus of primary concern.

Astronaut Observations on Descent

The reports of the Apollo missions hold some very valuable information regarding the dust disturbed by the landing of the lunar module (LM). During the first two lunar landings, the Apollo astronauts were amazed by great sprays of dust on descent (Apollo 12 Technical Crew Debriefings, 1969). First observed by Apollo 11 astronauts at about 25 m (82 ft), the streaking dust eventually resulted in a total loss of visibility by 2.7 m (9 ft) (Scott et al., 1970). This effect was so disorienting that later Apollo missions incorporated a quicker descent with a translational motion to maintain visibility (see fig. 9). Nonetheless, both Apollo 12 and 14 astronauts first observed dust at 33 m (108 ft) from the lunar surface (Mitchell et al., 1971). Actually, the dust easily reached 37 m if the 4-m distance from the LM observation windows to the footpad is included.

With the use of simple Newtonian projectile theory, the minimal initial velocity v_{0y} of these first particles can be estimated for the particle elevations observed. The initial velocity is

$$v_{0y} = \sqrt{2gy_{max}} = 11 \text{ m/s} \tag{7}$$

where g, the lunar surface gravitation constant, is 1.63 m/s^2, and y_{max} is 37 m.

It may be assumed that other particles are traveling with angled trajectories whose vertical component was initially 11 m/s. The maximum horizontal distance achieved by those particles moving at 45° would be

$$x = \left(v_{0y}\sqrt{2}\right)^2 \frac{\sin 2\phi}{g} = 148.5 \text{ m} \tag{8}$$

Consequently, when dust streaks are first at 33 m, a dust cloud exists below which is at least 297 m in diameter.

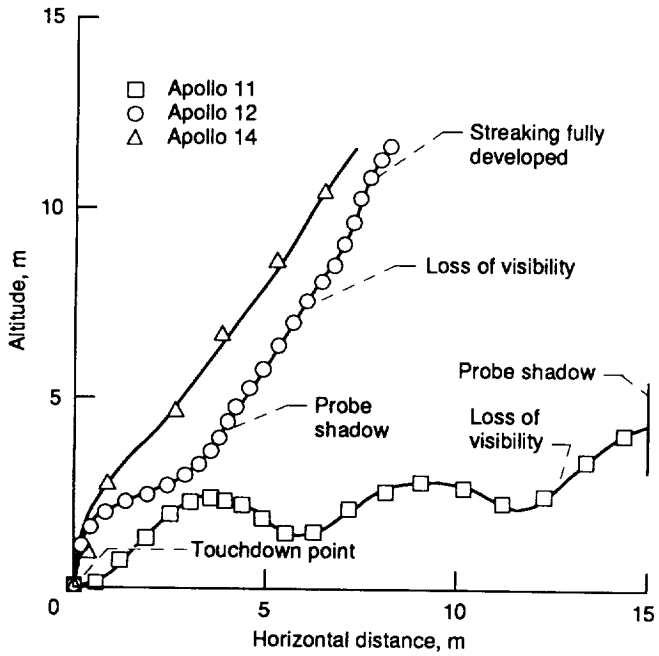

Figure 9.—A comparison of the final approach profiles of the Apollo 11, 12, and 14 lunar modules. Dust was first observed on the Apollo 11 at 25 m (64 s before touchdown), and on the Apollos 12 and 14 at 33 m (52 and 44 s before touchdown, respectively). The Apollo 14 was able to maintain visibility through touchdown (Mitchell et al., 1971).

As the LM continues to approach the surface, the engine blast focuses on a smaller and smaller area of soil. The dust particles reach greater velocities and, therefore, greater horizontal distances.

Although the laws of pure Newtonian motion are independent of particle size, particle ejection may be size-dependent. Any size sorting of lunar dust particles occurs in the momentum transfer between the exhaust gases and soil, and in the complex aerodynamic processes in the turbulent exhaust zone. Therefore, it might be reasonable to expect that larger particles do not travel as far or attain the velocities of very small particles. Once the particles are clear of this zone and experience only the vacuum of the lunar environment, however, motion is purely Newtonian. In the absence of atmosphere, there is no friction or drag or any other size-selective effect.

Apollo Erosion Scars

Other effects of the Apollo LM landings are the scars and grooving in the soil surface caused by engine blast. For each Apollo landing, a great erosion track traced the approach (fig. 10) and culminated in a shallow pit under the engine bell.

In the specific case of the Apollo 14, the surface erosion is visible in post-landing photographs taken with a low sun angle. The descent engine produced roughly 13 400 N (3000 lb_f) of thrust until 2 s after contact. The eroded area has a sandblasted roughness superimposed on a radial "grooving" pattern (figs. 11 and 12). The deepest area is displaced about 1 m from the center of the resting engine bell, where the LM momentarily hovered (Mitchell et al., 1971). This burn is estimated from the photographs to have a depth of 10 cm and a diameter of 220 cm; the edge is ill-defined, since particles far beyond this were also disturbed during descent. In any case, from this burn alone a bulk volume of approximately 444 liters (16 ft^3) was removed as calculated from the equation for the volume of a spherical segment of one base:

$$V_{ss} = \frac{h\pi\left(3r^2 + h^2\right)}{6} = 444\ 012\ \text{cm}^3 \tag{9}$$

The bulk lunar soil density increases with depth to a maximum of about 1.75 g/cm^3 below 60 cm. In the top 15 cm, the average bulk density is approximately 1.5 g/cm^3 (Carrier, 1990). Thus, 666 kg of soil was blasted from this burn.

The average mass of a lunar soil particle weighted to the probability of occurrence can be roughly estimated with the following relation:

$$m_{ave} = \int N(D)\left[m(D)\right]dx \tag{10}$$

The relative number of particles of each size $N(D)$ is developed in appendix B. In establishing the mass of each size particle, $m(D)$, the particles are assumed to be spherical for simplicity, and the material density is taken to be 3 g/cm^3 after Duke et al. (1970):

$$\begin{aligned} m_{ave} = \int_{1\,\mu\text{m}}^{1000\,\mu\text{m}} N(D)\left[m(D)\right]dD &= \int_{1\,\mu\text{m}}^{1000\,\mu\text{m}} \left(\frac{3}{D^4}\right)\left[\frac{3\text{g}}{\text{cm}^3}\left(\frac{\pi D^3}{6}\right)\right] \\ &\quad \times\left[\frac{100\ \text{cm}}{10^6\,\mu\text{m}}\left(\frac{10^6\,\mu\text{g}}{\text{g}}\right)\right] dD \\ &= \frac{3\pi\left(10^{-6}\right)}{2}\int_{1\,\mu\text{m}}^{1000\,\mu\text{m}} \frac{1}{D}dD \\ &= \frac{3\pi\left(10^{-6}\right)}{2}\ lnD\Big|_{1\,\mu\text{m}}^{1000\,\mu\text{m}} \\ &= 3.25\times10^{-5}\ \mu\text{g/particle} \end{aligned} \tag{11}$$

The 666 kg of lunar soil that was removed and dispersed from the region directly under the engine bell alone corresponds to a large number of particles:

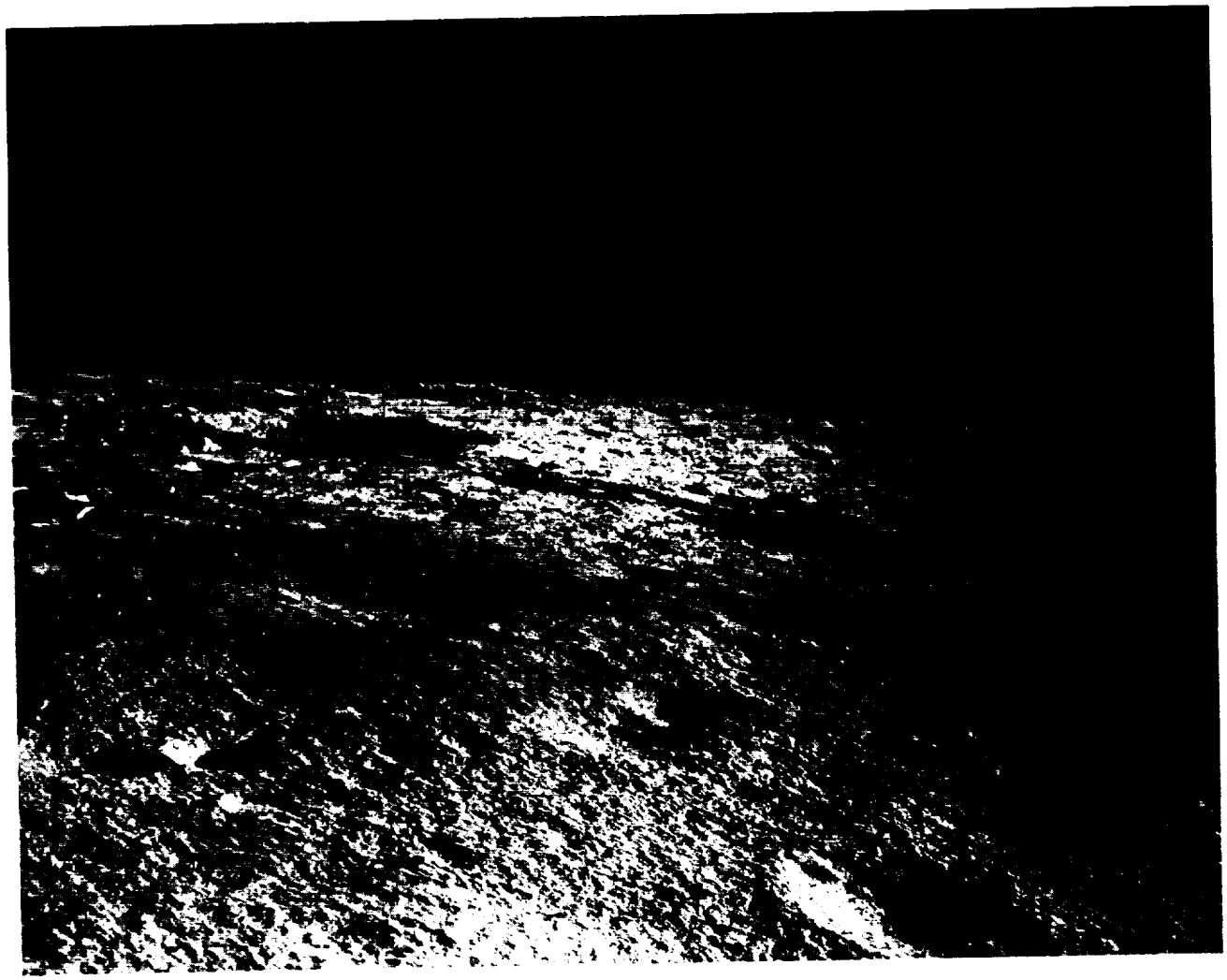

Figure 10.—Erosion track, 40 to 50 ft east of the Apollo lunar module landing site (AS12-46-6781).

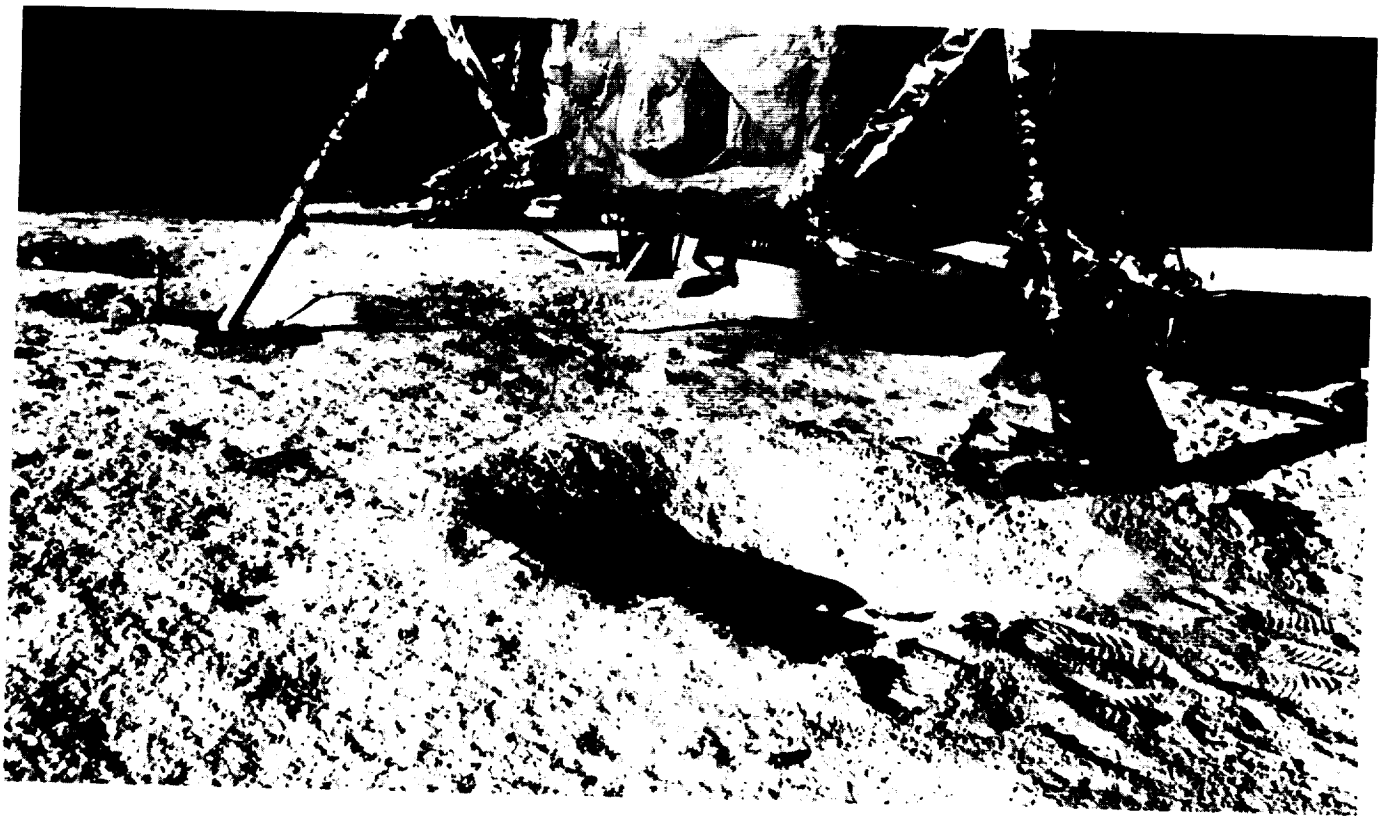

Figure 11.—Composite photograph showing the eroded area beneath the engine bell of the Apollo 14 lunar module (S-71-25423).

$$(666\ \text{kg})\frac{10^9\ \mu\text{g/kg}}{3.25\times10^{-5}\ \mu\text{g/particle}} = 2.05\times10^{16}\ \text{particles} \quad (12)$$

If these particles were distributed homogeneously over the region defined in equation (8) by a 148.5-m radius, the resulting deposition would be 9.6 g/m^2, or 3x10^{11} particles/m^2.

Surveyor III

The Surveyor III provides a singular opportunity to observe some of the effects of the landing of an Apollo LM. The Surveyors were a series of unmanned exploratory craft sent to develop soft-landing technology and to study the lunar surface environment prior to the Apollo missions. The Surveyor III, like the other Surveyors, was equipped with a special television camera to transmit images of rock formations, craters, and soil color and texture. In addition, the Surveyor III had a retractable shovel for performing impact tests, trench tests, and other manipulations of the lunar soil under camera observation (refer again to fig. 4) (Jaffe and Steinbacher, 1969; Milwitzky and Dwornik, 1967).

On April 20, 1967, the Surveyor III touched down in the eastern part of the Oceanus Procellarum. After two hops it came to rest on the inner edge of a 200-m crater later known as "Surveyor Crater." It transmitted 6326 pictures of the lunar surface before it became inactive on May 3, 1967, in preparation for lunar night, and has been silent ever since (Milwitzky, 1969).

Thirty-one months later, in November 1969, the Apollo 12 came to the same crater in the Oceanus Procellarum. One of its missions was to achieve a pin-point lunar landing at a preselected site. At the same time it afforded the opportunity for scientific evaluation of the long-term effects of the lunar environment on the Earth-made materials of the Surveyor III.

The Apollo 12 approached from the east, crossing the northern edge of the crater, and touched down on the northwest rim, 155 m (509 ft) away. (See fig. 13.) During its approach, the LM was as close as about 67 m above a point on the ground located roughly 109 m from the Surveyor.

During their second extravehicular activity (EVA), the Apollo 12 astronauts, Charles Conrad and Alan Bean, visited the Surveyor III to take photographs and to retrieve some of its components for later study. The following were removed with a pair of shearing cutters and returned in the Surveyor tote bag (Carroll et al., 1972a):

(1) The complete television camera with its associated optical, electronic, mechanical, and structural components
(2) The sampler scoop, with 6.5 g of adhering lunar soil
(3) A 19.7-cm section of unpainted aluminum tube from a sensor support strut
(4) A 10-cm length of aluminum tubing (painted with white inorganic paint) from the camera support strut
(5) A 13-cm length of television cable, with aluminized plastic wrapping

During the general inspection of these parts it became clear that almost all exposed surfaces were partially covered with

Figure 12.—Closeup photograph of the erosion caused by the exhaust plume of the Apollo 14 descent engine during touchdown (AS14-66-9261).

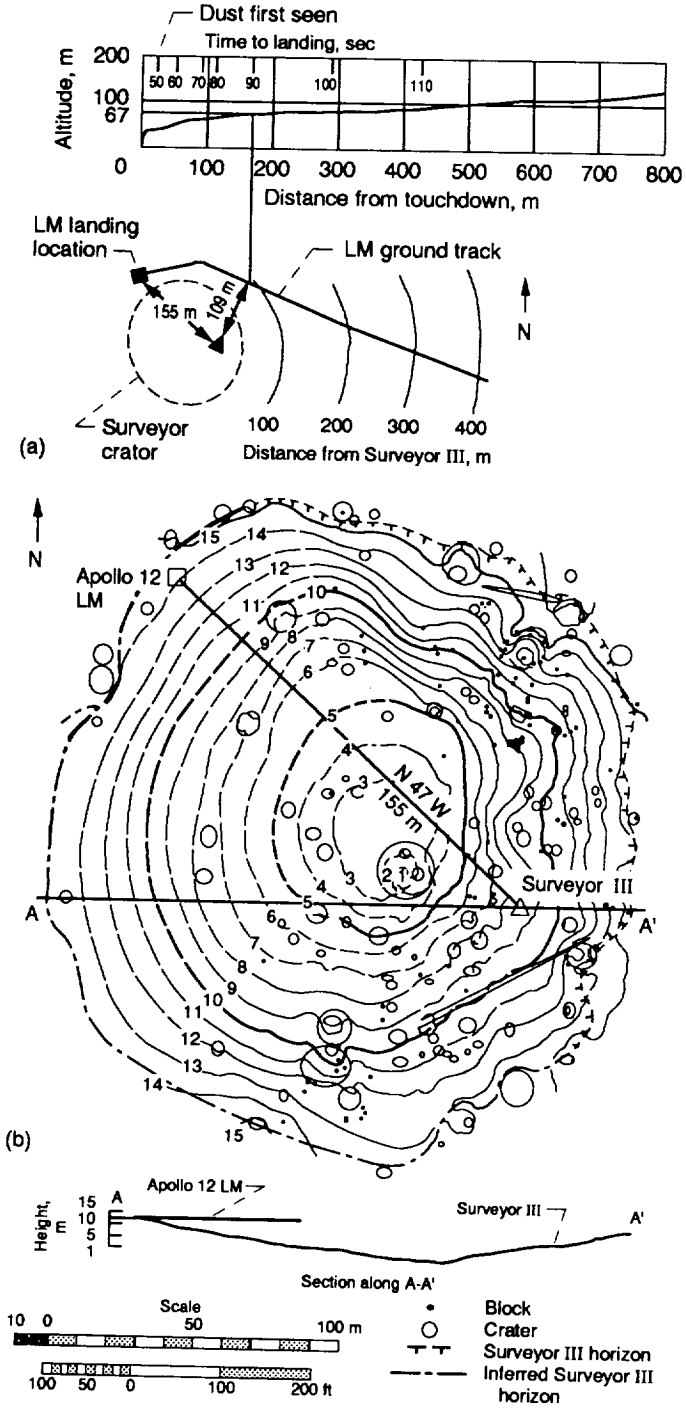

(a) Profile and plan view of the Apollo 12 approach and landing relative to the Surveyor III spacecraft. The closest point along the ground track was about 109 m while the lunar module (LM) was at an altitude of 67 m (Nickle, 1972).

(b) Plan and cross-sectional view of "Surveyor Crater" showing relative positions of the Surveyor III and Apollo 12 LM. The contour interval is 1.0 m, and dashed contour lines are approximate. The LM landed 155 m away from the Surveyor, at a ground level 4.3 m higher than the Surveyor television camera. (Data taken from Carroll, 1972).

Figure 13.—Apollo 12 LM landing site approach and site contour.

a fine layer of lunar dust. A small amount of this dust may be attributed to particles disturbed by the Surveyor's own vernier engines. Some may also have resulted from the abnormal Surveyor III landing in which the craft took two hops before coming to rest. However, in their summary of the findings of 40 investigative teams, Nickel and Carroll restate, "it has been demonstrated that more dust exists now than at the time of the Surveyor III mission." Moreover, there seemed to be no evidence of natural transport processes. Therefore, it was concluded that the main source of lunar dust was necessarily the landing of the LM nearby. (Nickel and Carroll, 1972).

Considerably more dust was found on the retrieved Surveyor III components than was previously expected. Although the distribution over the entire craft was not homogeneous, it was generally observed that the LM—and leeward—sides of the Surveyor III had about the same amount of lunar dust (Carroll et al., 1972b). This suggests that a huge nondirectional cloud of disturbed dust accompanied the first stages of approach, covering the Surveyor indiscriminately with a dusting of particles. More particles accumulated on the northern side as the LM continued its descent, but were then eroded by the directed blast of the final approach.

Of the components returned, the television camera unit provides the most complete evidence for dust transport by the LM engine blast. It consisted of a vertical camera with a rotating carousel of light filters above it (fig. 14). The object's image was reflected by a large moveable oval mirror down through the filter and into the camera, where it was converted and transmitted. The whole unit was housed in a protective metal hood and collar, located on the northeast side of the Surveyor III, facing somewhat away from the LM landing site.

In the most cursory inspection with the unaided eye, a directional darkening or shadowing was visible behind each raised feature on the northwest surface of the camera hood (fig. 15). These "shadows" corresponded to direct projections of cables and bolt heads, and other features originating from the LM landing site. This effect is explained as "sandblasting" by lunar material that had become entrained in the engine exhaust gases, lightening the surfaces by removing material and leaving dark shadows where protected (Carroll et al., 1972b). Even the camera mirror was eroded by sandblasting.

More evidence of the sandblasting effect was found in the organic contamination analysis of the camera's exterior surfaces and mirror. The organic LM descent engine products—distinct from the Surveyor's vernier engine products—were twice as concentrated on the leeward surface than on the surface facing the LM (Carroll and Blair, 1972). This is consistent with the hypothesis that the LM first disturbed a great diffuse cloud of dust which engulfed the entire area and then eroded material from the northern surfaces on its final approach.

During their initial survey of the condition of the Surveyor III, the Apollo 12 astronauts paused at the hazy oval object

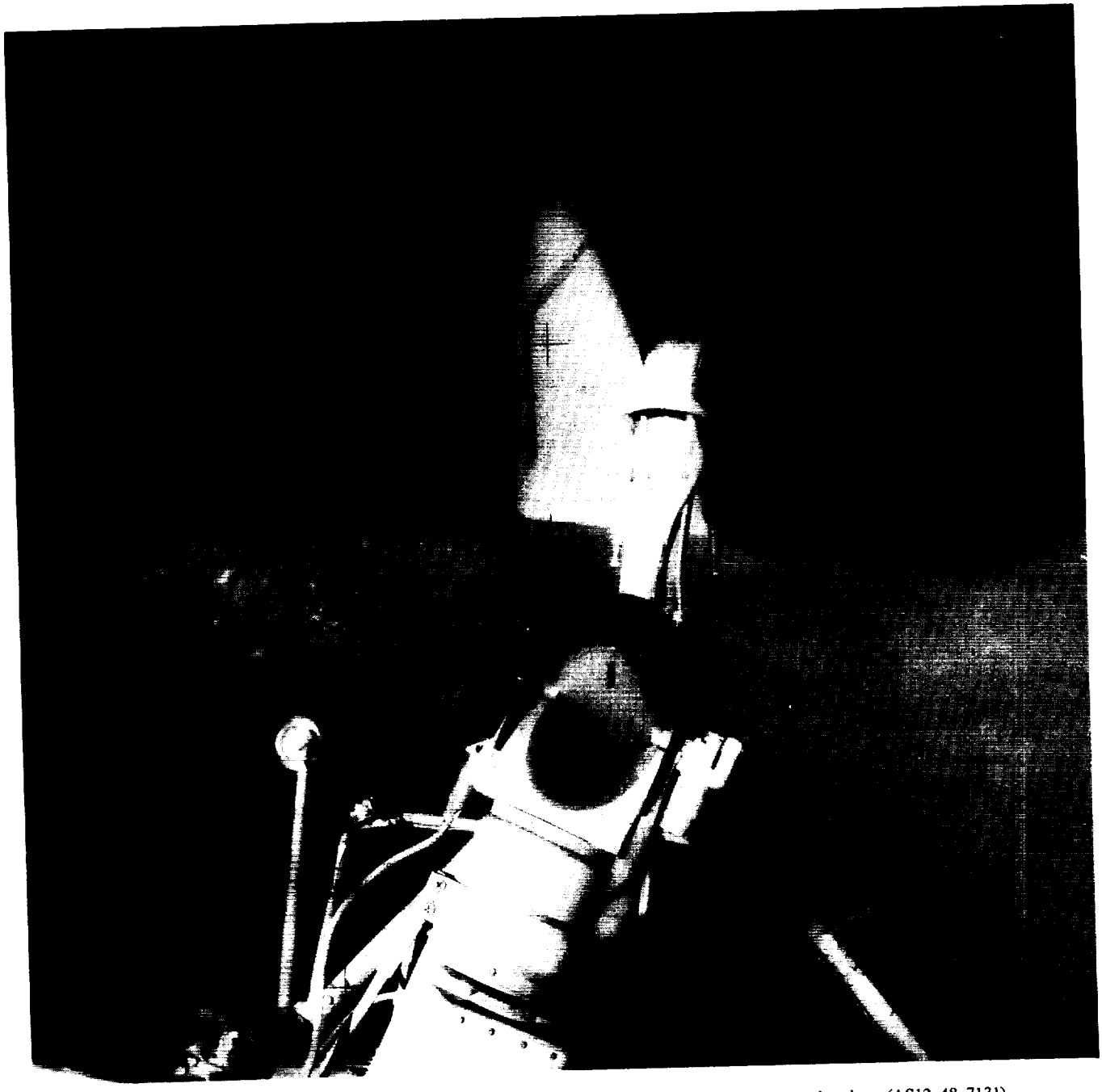

Figure 14.—Surveyor III camera. The finger swipe of astronaut Conrad is visible in the camera's mirror (AS12-48-7131).

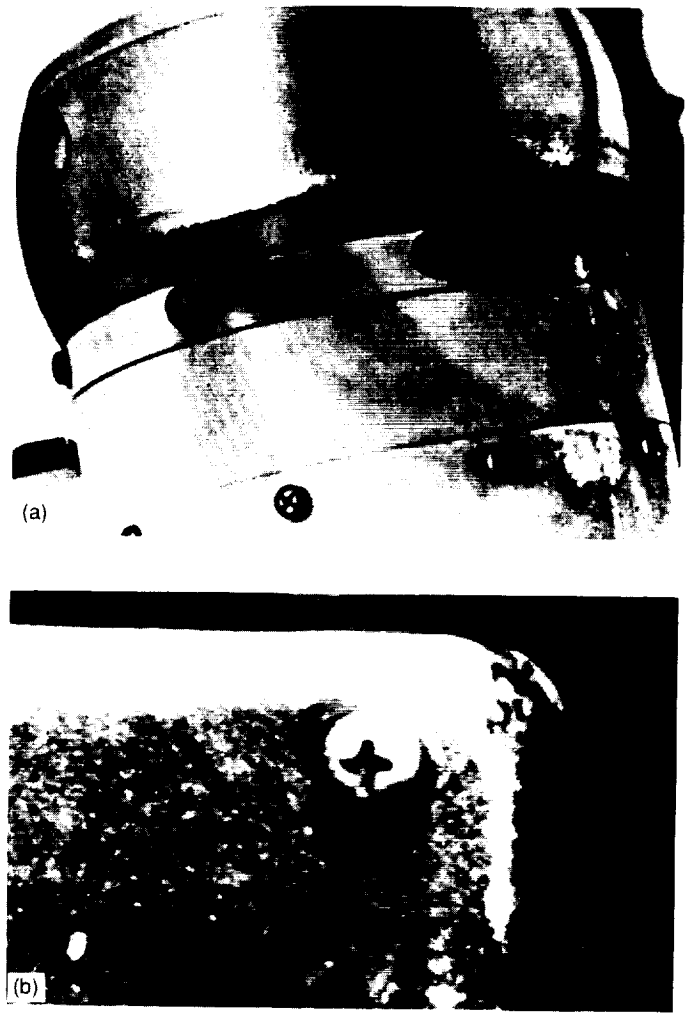

(a) Various camera attachments and cables.
(b) Closeup of a bolt head.

Figure 15.—Evidence of particle impact shadows on the Surveyor III television camera housing. (Data taken from Cour-Palais et al., 1972.)

they thought should be the shiny camera mirror. With a wipe of a gloved finger, they saw the smooth reflective surface they expected beneath a layer of lunar dust. (Refer again to fig. 14; also see fig. 16.) It has since been established that the primary cause for the "veiling glare" and contrast attenuation in the returned mirror is the presence of lunar dust on its surface (Carroll et al., 1972b). Erosion and organic contamination are very minor contributors.

Because of the angled final resting attitude of the mirror, its dust coverage is smoothly graded—heaviest at the top and lightest at the bottom. The lunar material was removed with successive "peels" of an acetate replicating tape for analysis. Except for a rare fleck of Earth-origin, all particles conformed to the elemental, mineralogical, and morphological characteristics of lunar soil. Particles between 0.3 and 3 μm account for almost 90 percent of the total mass of dust accumulated on the mirror surface. Very few particles were found which were greater than 4 μm (Carroll et al., 1972a, 1972b; Rennilson, Holt, and Moll, 1972).

The camera filter wheel was recessed in the hood collar. Nevertheless, it was also covered with a dust, which resulted in a transmittance loss of 25 percent (Nickel and Carroll, 1972). Mathematical interpretations predict a surface dust coverage of 25 percent (Carroll and Blair, 1972). Here the particles size of the lunar fines ranged from less than 1 μm (approximately 50 percent of the particles) up to 40 μm (Nickel and Carroll, 1972). From reflectance data and filter transmittance measurements, it is estimated that 10^{-5} to 10^{-4} g/cm^2 of lunar material was deposited on these filters as a result of the landing of the LM 155 m away (Carroll and Blair, 1972).

Various regions of the painted camera hood were analyzed for dust coverage. The composition profiles produced by sputter-ion source mass spectroscopy indicate that a dust layer as thick as 8.7 μm accumulated on the visor top, and a 7.2-μm layer was deposited on the lower section facing the LM (Satkiewicz and Marmo, 1972). Overall, Carroll and Blair estimated that no less than 10^{-3} g/cm^2 of lunar soil arrived at

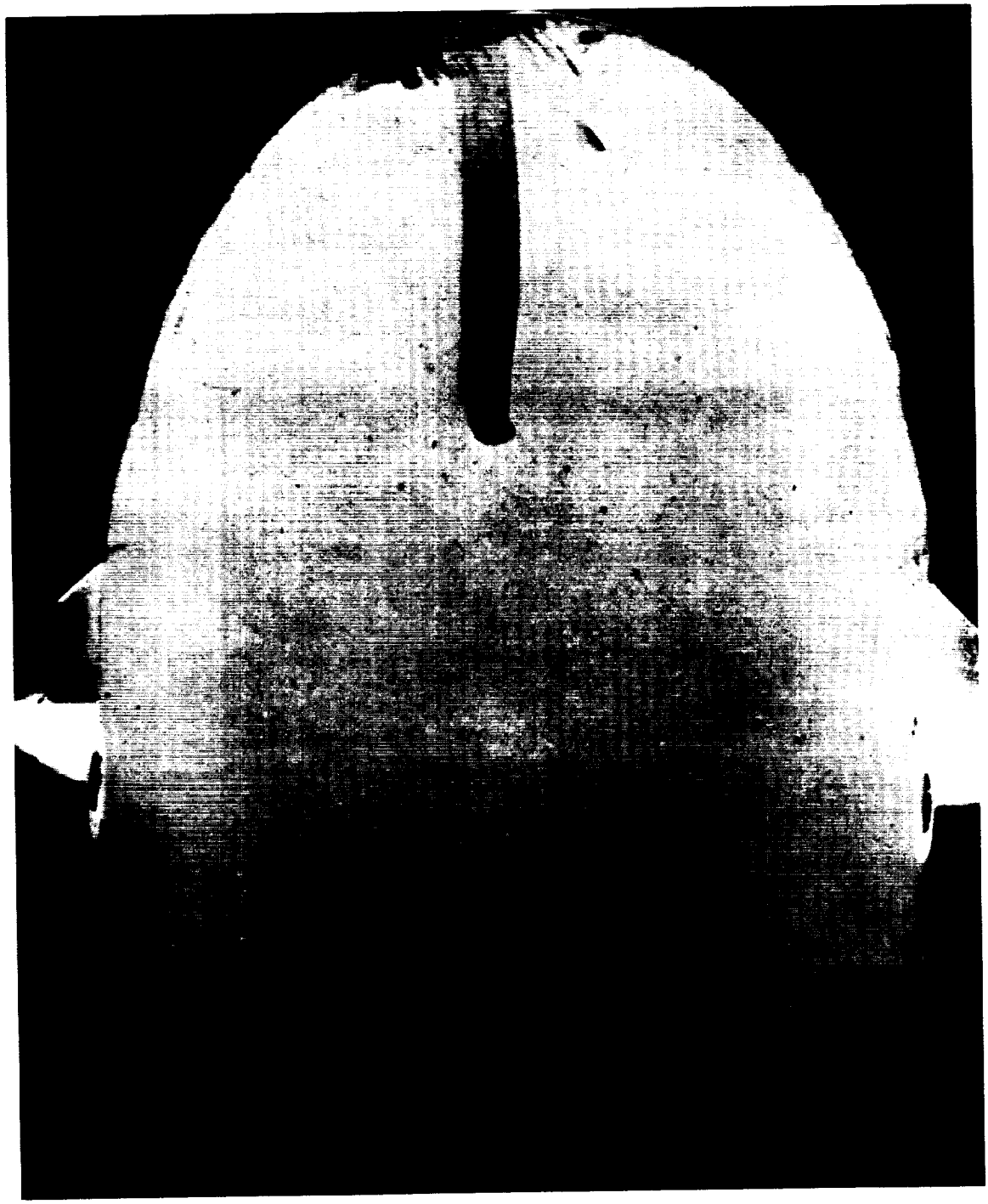

Figure 16.—Surveyor III television camera mirror showing a coating of fine-grained lunar material covering its entire surface. The finger swipe was made by astronaut Conrad prior to its removal and return (Nickle, 1972).

the Surveyor III, though some merely sandblasted instead of accumulating (Carroll and Blair, 1972).

Under microscopic evaluation many types of microcraters or pits were observed on a variety of surfaces. None of these pits has been positively identified as the result of hypervelocity micrometeoroid impact (Carroll et al., 1972a). Some pits found on painted aluminum tubing were attributed to pores in the coating, which are not a function of the lunar environment (Anderson et al., 1972). On the glass optical filters, the deepest pits were consistent with the manufacturing and polishing techniques (Brownlee, Bucher, and Hodge, 1972). However, of those pits that were attributed to the Surveyor's tenure on the Moon, most were traced to the impact of dust particles excited by the LM descent. The presence of lunar material was confirmed by detection of Ca, Ti, and Fe in the pits (Anderson et al., 1972). Also, the direction of impact correlates with the LM approach and descent.

By the shadowing of screwheads, cables, and other hardware, it was clear that the majority of the dust generation occurred at touchdown, that lunar particles were ejected almost horizontally, and that the trajectories were well-collimated. One group of investigators estimated an average particle velocity of approximately 40 m/s based on the alignment of the shadows with the LM location (Nickle and Carroll, 1972). Jaffe predicted 70 m/s, also by the crisp shadows on the camera housing (Jaffe, 1972). Another group judged the dust velocity to be in excess of 100 m/s—their conclusion considered the dust trajectory to be only slightly affected by lunar gravity (Cour-Palais et al., 1972).

Since these estimates describe the *average* particle velocities during final descent as interpreted by the markings on the Surveyor 155 m away, it is likely that particles may have been traveling considerably faster than this. Particularly those particles which experienced the direct engine blast are candidates for much greater velocities. The camera's smooth optical filters provided a special opportunity to refine an upper limit on the particle velocities. These filters did not have a direct view of the landing site, and yet it was observed that particles impacted with even distribution over their 160° field of view. The result was an average filter pit density of 200 pits/cm^2 of the size 0.5 μm to 10 μm. (This corresponds to an impact rate of 800 impacts/cm^2-yr-(2π sr)—this is 1000 times greater than the rate expected for primary micrometeoroids (Nickel and Carroll, 1972).) Consequently, Brownlee's team concluded that most of these impacts resulted during the transverse east-west approach of the LM (during which the closest distance was 109 m at a height of 67 m) (Brownlee, Bucher, and Hodge, 1972). They determined that in order to produce the observed fractures in the glass surface, a 1-μm particle must have impacted with a velocity of roughly 2 km/s or more. By the pit characteristics—irregular depressions or dents with signs of plastic flow and chipped rims—the incoming particle velocity was therefore appraised to be in the range 0.3 to 2 km/s (671 to 4470 mph), a conservative estimate of later touchdown conditions. The pit shape was consistent with the necessarily low angle of impact to reach the partially protected filters. In addition to the impact angle, the initial ejection angle must also have been at, or slightly below, the horizontal, since the Surveyor III camera was roughly 5 m below the rim of the crater (Brownlee, Bucher, and Hodge, 1972). Therefore, the dust disturbed during the final touchdown would be expected to have at least a comparable velocity and degree of collimation.

Prior to the Apollo 12 mission, it was generally assumed that 500 ft would be a sufficient distance to land one craft without affecting another. However, one of the unanimous conclusions of the many investigators who studied the returned Surveyor components was that dust is a considerable factor at these distances. They emphasize that this issue must receive future attention because the presence of dust, even in small amounts, can significantly affect the thermal control and optical performance of critical hardware.

Dust Accumulation From Spacecraft Landing and Launch

Modeling Accumulation Distributions for Spacecraft Landing

From the previous sections it is clear that large amounts of lunar dust are suspended by the descent (and probably ascent) of a spacecraft on the lunar surface. This dust travels fast and far, and accumulates indiscriminately on nearby surfaces. The magnitude of dust accumulation with distance from a landing event is of critical importance in the prediction of photovoltaic array and radiator performance.

Even with the Apollo and Surveyor experiences with lunar dust, expected dust accumulation remains an elusive and difficult quantity to establish. This is largely due to the sandblasting effects of final touchdown which removed some of the dust acquired on Surveyor III surfaces during the earlier stages of LM approach and descent. Consequently, a value for the total amount of dust arriving at a certain distance is impossible to obtain. In addition, because of the complex disturbance processes, particle trajectories are myriad. Dust accumulation as a function of the distance from a landing site may only be projected from the available information from these missions, and extrapolated as well as possible to future lunar base scenarios.

To prepare a base model for dust accumulation as a function of distance from the LM, the clues available from the Surveyor components were cut and pasted together to generate a model for particle velocity distribution. The velocity distribution was converted to a particle distance distribution, which was summed over the possible range of angles to arrive at an accumulation with distance. Finally this accumulation distribution was scaled to correlate with the observed accumulation on the Surveyor III.

The Surveyor evidence indicates that most particles disturbed during touchdown have a velocity between 40 and 100 m/s at a distance of 155 m from the landing site of an Apollo LM,

with an average velocity of 70 m/s. There are also particles which arrive in excess of 2000 m/s, producing the observed pitting in glass surfaces. From the shapes of these pits and the "shadowing" of bolts and cables, it was deduced that the trajectories were well-collimated at an angle of approximately 0°. This may be an understatement of the disturbance caused by the LM's final touchdown, the stage of descent when the particles are ejected with the greatest energy under the direct blast of the descent engine. Nevertheless, it is a reasonable place to start in the absence of more data.

From this information, three velocity distributions were generated. All are normal, bell-curve distributions of the form

$$N(v_0) = C \exp\left[-0.5\left(\frac{v_0 - \beta}{\sigma}\right)^2\right]$$

where v_0 is the ejected particle velocity, and β, the mean value, is taken to be 70 m/s. In model 1, the standard deviation σ is assigned to be 500 m/s, which corresponds to the case when as many as 1 in 10 000 particles travels at a velocity greater than or equal to 2000 m/s to account for observed pitting. The associated curve is very flat, and less than 5 percent of model 1 particles fall in the range 40 to 100 m/s (see fig. 17). A standard deviation of 100 was selected for model 2. This describes the case in which a greater fraction of all particles, (23.6 percent) fall between 40 and 100 m/s, but less than 0.001 percent are faster than 2000 m/s. For comparison, model 3 was assigned to have a standard deviation of 44.8, which would correspond to a population in which 50 percent of the particles had a velocity between 40 and 100 m/s (the observed velocity range), and much less than 0.001 percent had a velocity of 2000 m/s or greater. Table II summarizes the differences among the three models. Of these, model 2 may be the best simulation of the actual scenario as described by the Surveyor components; if the real distribution were as "flat" as model 1, it is unlikely that the three groups of investigators would all have estimated the average velocity to be within 60 m/s of each other. Also, model 1 predicts the greatest number of fast particles, which would have produced more damage than observed. In the other extreme, it does not seem reasonable for the particle velocity to be as sharply defined as predicted by model 3.

The velocity distributions were normalized over distance values from zero to infinity, assuming radial symmetry around the LM. From the laws of Newtonian motion, values of velocity can be converted to distance by

$$v_0 = \sqrt{\frac{xg}{\sin 2\phi}} \qquad (13)$$

Here ϕ is the ejection angle and g, the lunar gravitation, is 1.63 m/s^2. Since the particle trajectories are known to be nearly horizontal, ϕ values from 0° to 1° were considered. The result is a series of distributions—each describing the number of particles that travel distance x for a given ϕ—of the form

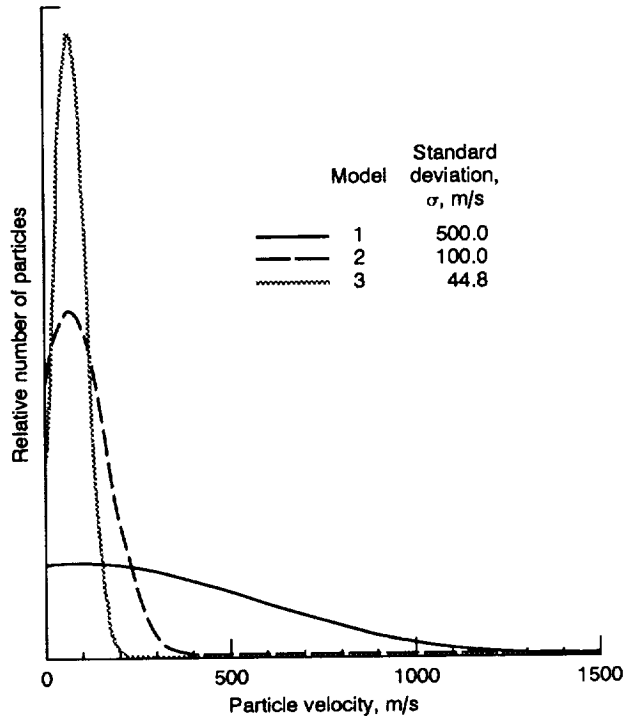

Figure 17.—Three models of the particle velocity distribution of lunar dust distributed by the final touchdown of the Apollo lunar module.

$$N(x) = C \exp\left[-0.5\left(\frac{\sqrt{\frac{xg}{\sin 2\phi}} - 70}{\sigma}\right)^2\right] \qquad (14)$$

An example for model 2 is shown in figure 18, where the curves for three different angles are plotted and normalized for all positive x. They, therefore, give only the *relative* number of particles with distance. They illustrate, however, the great sensitivity of the distribution to ejection angle; particles ejected with ϕ = 1° travel roughly 2 orders of magnitude farther than those with ϕ = 0.01°.

Finally, the relative number of particles was summed over 100 angles between 0° and 1° to give a total number of particles arriving at each distance. The total number of particles was then modified to number per square centimeter by the multiplication of a constant. Another constant converted number of particles to mass in milligrams per square centimeter. The constants are not really critical, since the last step required scaling the curves, one for each model, to intersect the value

TABLE II.—PARTICLE VELOCITY DISTRIBUTION MODELS FOR NORMAL DISTRIBUTION

[Mean velocity, β, 70 m/s]

Model	Standard Deviation σ, m/s	Probability of velocity of 40 to 100 m/s, percent	Probability of velocity greater than 2000 m/s, percent	Particle velocity distribution function, $F(x)$, after normalization
1	500	4.78	< 0.01	$0.00143 \exp [-(x-70)^2/500\,000]$
2	100	50	<< 0.001	$0.00945 \exp [-(x-70)^2/2000]$
3	44.8	23.6	<<< 0.001	$0.00524 \exp [-(x-70)^2/4014]$

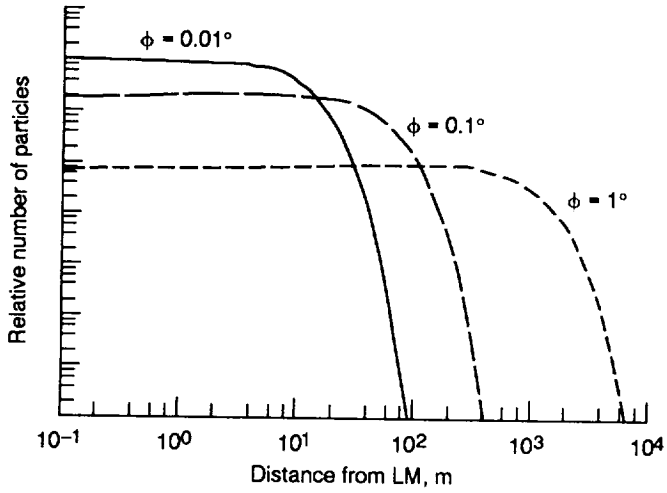

Figure 18.—Particle distance distribution of lunar dust distributed by the final touchdown of the Apollo lunar module as predicted by model 2. The distribution's dependence on ejection angle ϕ is significant: the maximum distance can vary by roughly two orders of magnitude between ϕ = 0.01° and ϕ = 1°. Since the curves are normalized over all distance, actual accumulations cannot yet be determined.

1 mg/cm^2 at 155 m. Recall that this is the estimated amount of dust remaining on the Surveyor. Because this value does not account for particles that were sandblasted away, the curves (shown in fig. 19) are likely to underestimate the net accumulation through this scaling process. Nevertheless, the models show in a general way that after experiencing several lunar landings a surface could easily acquire a substantial amount of dust.

In figure 19 the accumulation curves peak at a distance near 100 m from the landing site. This peak may be attributed to the contribution of those particles ejected at very low angles. Beyond this peak, the accumulation curves drop off exponentially, according to equation (14). Model 1, which has a very large standard deviation, predicts an enormous accumulation even at 10 km, whereas model 3 predicts the accumulation at that distance to be essentially negligible. At 1 km, the accumulation according to models 1, 2, and 3 are 0.83, 0.14, and 0.001 mg/cm^2, respectively. As mentioned, model 2 represents the most reasonable interpretation at this time, but it bears confirmation by more lunar data.

It is interesting to note that the Moon's escape velocity is 2.3735 km/s. Therefore, by any model, every landing will launch some lunar particles into orbit. This also means that even surfaces that are quite far away from a landing event may experience reduced performance due to dust accumulation.

In addition to traveling great distances, the faster particles can also inflict surface damage in the form of impact pits. Unfortunately, such particle trajectories are not moderated by flight through a gaseous environment as they are on Earth. However, it is not clear whether these pits will necessarily degrade performance. For photovoltaic arrays, provided the protective cover-material is thick enough to prevent solar cell damage, a roughened surface may still allow nearly normal performance via diffuse rather than specular solar

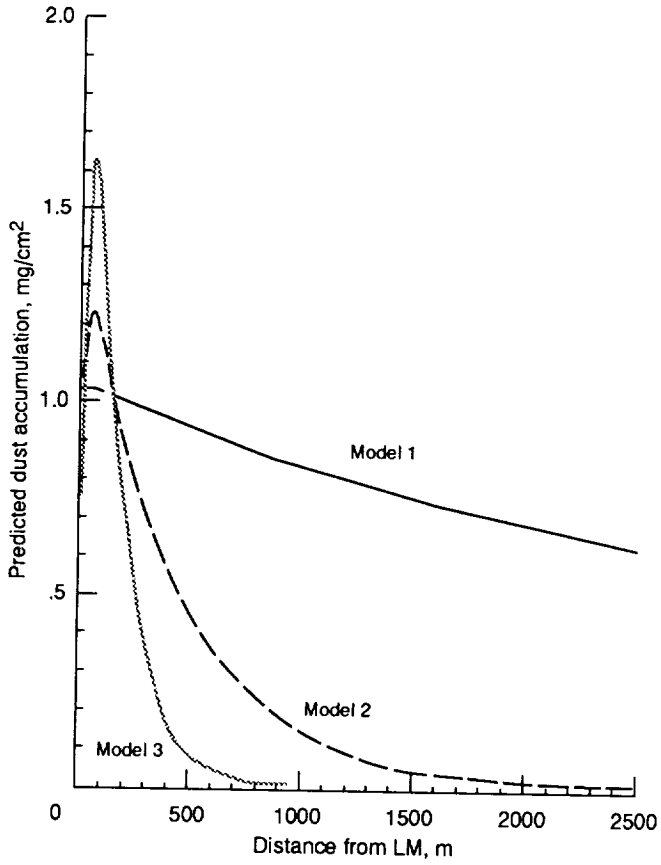

Figure 19.—Estimated lunar dust accumulation resulting from the lunar module final touchdown. These curves were all scaled to have the value of 1 mg/cm^2 at a distance of 155 m from the landing site, which is the best available estimate from the Surveyor III returned components.

illumination. In the case of radiators, special high-emittance surface coatings may be eroded—or conversely, the roughening may provide additional surface area, such as achieved through arc-texturing techniques (Banks et al., 1988). For either surface, the more definite problem appears to be occlusion from incoming or outgoing electromagnetic radiation by a coverage of particles.

Independent Predictions of Particle Trajectories and Fluxes for Spacecraft Landing

Under a contract for NASA Johnson Space Center, Eagle Engineering, Inc., evaluated the factors that needed to be considered in the planning of a lunar launch and landing facility. Among the issues discussed in their reports was the tossing of lunar dust by the exhaust plume (see Phillips et al., 1988, and Lunar Base Launch & Landing Facility Conceptual Design, 1988). Using a 50 000-N LM-type engine as a baseline model, they predicted the sizes, trajectories, and fluxes of the lofted particles by assessing the direct drag acceleration by the plume. Though the nature of the calculations were not included in their reports, the results are worthy of mention as an independent evaluation of particle accumulation.

Table III shows a summary of some of the predictions made by the Eagle group. As an example, they anticipated a 50-μm particle to travel 2 km and impact with a velocity of 125 m/s. By their analysis, larger particles do not travel as far, or attain such velocities. Particles greater than 5 mm are too large to be ejected by the plume.

The Eagle group estimated particle flux by calculating the number of 50-μm particles needed to produce a 50-percent obscuration. By their model, at 1 m roughly 0.1 impacts are expected per cm^2-s (see fig. 20); the final 10-m descent of a typical landing event may last 5 s. For larger particles, the flux is lower. This is reported as a conservative estimate. From these results, Phillips et al. predict that surfaces within 200 to 400 m would receive substantial pitting from a 50 000-N descent engine and that glass surfaces, in particular, would be rendered "unusable." They predict that after one landing, glass objects 2 km away will sustain only 0.1-percent surface pitting, but that this could worsen to a noticeable haze after numerous landings (Lunar Base Launch & Landing Facility Conceptual Design, 1988). Although these results do not provide a direct estimate of the accumulation, they give the general idea that, under the influence of a 50 000-N engine, a measurable number of particles will reach surfaces at distances of 2 km.

Estimating the Effects of Spacecraft Launch

Launch is generally a quicker process than landing, since after an explosive burst of propellants the lunar surface is left quickly behind in contrast to a gradual controlled entry. Also navigation and orientation are not involved in launch until the later stages. Therefore, the exposure of the surface to direct

TABLE III.—ESTIMATED PARTICLE SUSPENSION BY A 50 000-N LM-TYPE ENGINE (Eagle Engineering, Inc., 1988)

Particle diameter, mm	Impact distance, m	Impact velocity, m/s
4.0	20	10
2.0	40	15
1.5	50	20
1.0	75	25
0.5	150	35
0.25	325	50
0.075	1200	100
0.050	2000	125

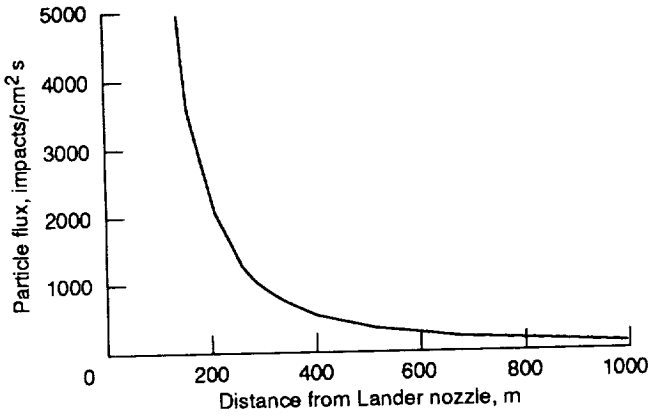

Figure 20.—Predicted particle flux distribution for a 50 000-N lunar-module-type engine for 50-μm particles (Eagle Engineering, Inc., 1988).

engine blast occurs over a shorter period. For two equivalent engines of the same dimension and thrust, the launch engine may be assumed to suspend less dust than the landing engine. However, the thrust levels required for launch are typically greater than those for landing, since braking against momentum and gravity is less energy intensive than accelerating from rest to above escape velocity. These inequities complicate the comparison. In addition, nozzle diameter and height also play a role in the degree of exposure of soil to exhaust gases. For instance, in the case of the Apollo launches, the lower portion of the LM consisting of the descent propulsion system and the landing gear was left behind, after serving as a launchpad from which to lift off. Consequently, the soil was not as directly exposed to the exhaust blast during ascent. The design of future lunar excursion vehicles has not yet been established to determine if such protection would be present. Apollo launch footage available from cameras that were left behind on the lunar surface shows dramatic streaks extending horizontally from under the plume. The particles are obviously moving with great velocities. Considering that the ascent engine produces greater thrust over a shorter exposure, the net number of particles suspended during launch and landing *may*

have been comparable in the case of the Apollo missions. For future missions, engine design—both thrust and physical dimensions—will determine whether launch or landing will cause more severe lunar dust suspension.

Scaling to Other Engine Thrusts

According to the Eagle group, an increase in thrust is directly proportional to an increase in the distance that disturbed particles will travel. Using this relationship, one can extrapolate both the authors' models and the Eagle models to other descent engine situations. For example, for a final touchdown thrust of 13 400 N, which was nominal for the Apollo LM's (Hammock, Currie, and Fisher, 1973), the Eagle model would predict that 50-μm particles would travel 536 m.

Similarly, the authors' models 1, 2, and 3 may be scaled to describe the particle accumulation for different descent engine sizes. Table IV shows the anticipated thrusts for "excursion vehicle" engines currently under consideration for servicing a future lunar base (B.A. Palaszewski, 1990, Launch Vehicle Research Branch, NASA Lewis Research Center, Cleveland, OH, personal communication). In equations (13) and (14), x would be multiplied by the appropriate ratio of new thrust to 13 400 N in order to correct for engine size. The particle distance distribution would accordingly stretch along the distance axis. In addition, a greater number of particles would be disturbed by a higher thrust engine. Since flux is related to the square of distance, flux is also related to the square of thrust. Therefore, the entire right side of equation (14) is squared. The result is an equation describing the anticipated dust accumulation resulting from a single landing of a modern excursion vehicle. For the sake of simplicity, it may be assumed that the same particle flux and accumulation distribution result from the launch of this vehicle, even though the thrust is greater. With the adoption of a possible schedule of base service missions, the accumulation distribution can be plotted as a function of time.

TABLE IV.—ANTICIPATED THRUST LEVELS FOR FUTURE LUNAR EXCURSION VEHICLES

	Apollo LM N_2O_4/hydrazine and [a]UDMH	Proposed O_2/H_2 propulsion	Proposed O_2/Al propulsion
	Thrust level, N		
Descent	[b]13 400	[c]26 800	[c]18 000
Ascent	[d]15 600	[c]76 000	[c]420 000

[a]Unsymmetrical dimethylhydrazine.
[b]Hammock et al., 1973.
[c]B.A. Palaszewski, 1990, Launch Vehicle Research Branch, NASA Lewis Research Center, Cleveland, OH, personal communication.
[d]Humphries and Taylor, 1973.

Lunar Dust Accumulation With Time

Consider a hypothetical scenario: the construction of the lunar base is complete, and though the base is largely self-sufficient, service missions from Earth are required twice a year to deliver necessary materials for maintenance of crew and facilities. The excursion craft uses O_2/H_2 propulsion, which provides 26 800 N of thrust on landing at the lunar surface. (This is twice the thrust of an Apollo LM descent engine.) It is supposed that an equivalent dust disturbance is generated during launch as is produced on landing, even though the ascent thrust levels are on the order of 76 000 N. After 5 yr, then, effectively 20 such craft have landed at the base. The resulting dust accumulation distribution therefore has the form

$$N(x) = 20C' \left[\exp \left(\frac{\sqrt{\frac{2xg}{\sin 2\phi}} - 70}{\sigma} \right)^2 \right]^2 \qquad (15)$$

Equation (15) is plotted in figure 21 for models 1, 2 and 3. According to model 2, the most representative interpretation, objects 1 km from the landing site will acquire a dust coverage of 3 mg/cm^2 after 5 yr. Figure 22 indicates, more generally, the dust accumulation distribution as a function of time for a number of different distances from the landing site for this same scenario. In short, it is clear that greater engine thrusts and multiple landings lead quickly to increased particle accumulations.

Correlation of Dust Accumulation and Power Component Performance

Radiator Performance

Using a simple model, one can compare the power radiated from a dust-covered radiator with that from a clean one (fig. 23). Consider an ideal case in which there is no competing absorption of solar radiation by either the radiator or the dust layer (for example, let the radiators in question be vertical, oriented along the Moon's equator). As a crude simplification, it is assumed that the interface between the radiator and dust layer is ideal, such that the first monolayer of particles receives heat from the radiator surface with 100-percent efficiency. To penetrate through the rest of the dust layer, the heat is both conducted across contacting particle surfaces and radiated from particle to particle. A thermal gradient will exist across the dust layer, and the radiation of heat into space will be limited by the resulting temperature at the dust surface. It is assumed that the dust accumulated on the radiator surface is not compacted, similar to the top

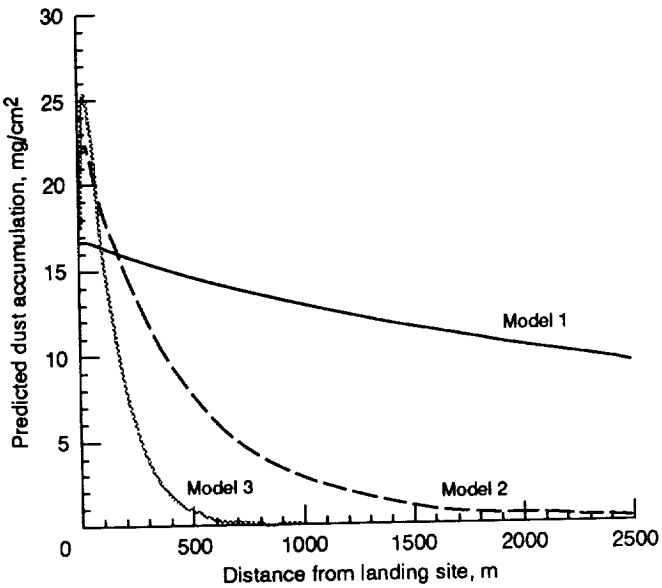

Figure 21.—Predicted lunar dust accumulation distribution resulting from launch and landing of lunar excursion vehicles with twice the thrust of the Apollo lunar module (26 800 N) over a 5-yr period of normal base operation. Models 1 to 3 are modified assuming that two service missions are required each year and that the dust profile from launch is equivalent to that from landing. It has also been assumed that thrust is directly proportional to distance and proportional to the square root of particle flux. Model 2 is believed to best represent the actual dust accumulation.

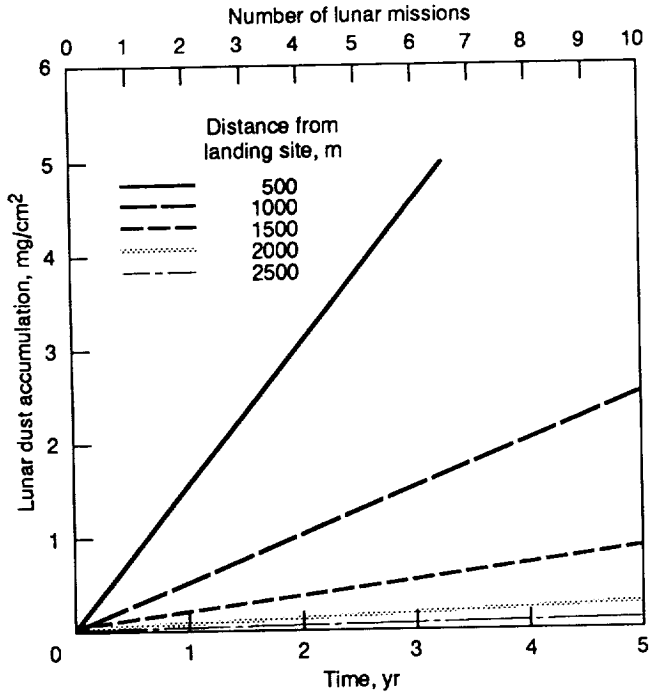

Figure 22.—Lunar dust accumulation distribution resulting from launch and landing of a 26 800-N lunar excursion vehicle as a function of time. Model 2 has been used to predict accumulation as a function of time at several distances from the landing site.

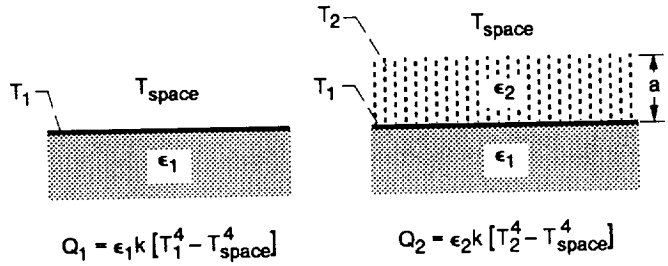

a	dust layer thickness, m
k	Boltzmann constant, W/m^2K^4
Q_1	heat flow per unit area from a clean radiator, W/m^2
Q_2	heat flow per unit area from a dust-covered radiator, W/m^2
T_{space}	effective temperature of space, K
T_1	temperature at the radiator surface, K
T_2	temperature at the surface of the dust layer, K
ϵ_1	emittance of radiator material
ϵ_2	emittance of lunar dust

Figure 23.—Comparison of a clean and dust-covered radiator surface.

few centimeters of soil on the lunar surface. As part of the Apollo 17 ALSEP experiment, Keihm and Langseth determined the thermal conductivity of the surface soil K_{eff} to be 1.5×10^{-3} W/m-K (Keihm and Langseth, 1974). In this experiment, specially designed thermocouples monitored soil temperature at various depths throughout the lunar day. By the nature of the measurement, the radiation of heat between particles was automatically included in the thermal conductivity. The ratio of thermal radiation to conduction was estimated to be 2.0 at 350 K. Because of this large radiation component, the thermal conductivity of lunar soil is not constant with temperature. Radiator temperatures of interest are considerably higher than 350 K: for the SP-100/Stirling engine system, the radiator operates between 525 and 600 K; for the SP-100/Brayton cycle system, the radiator temperature ranges from 700 to 900 K. Therefore, this temperature dependence must be incorporated. A simple approximation was confirmed for lunar soil (Cremers and Birkebak, 1971) and invoked by Langseth, Keihm, and Chute (1974) to break the effective thermal conductivity K_{eff} into its components of conduction K_c and radiation K_{Rad}:

$$\left.\begin{aligned} K_{eff} &= K_c + K_{Rad}T^3 \\ 1.5\times10^{-3}\ \mathrm{W/m-}K &= K_c + K_{Rad}(350)^3 \end{aligned}\right\} \quad (16)$$

where T is the material temperature in kelvin. Using the ratio from equation (16) as a second equation, one can determine the constants K_c and K_{Rad}:

$$\left.\begin{aligned} \frac{K_{\mathrm{Rad}}(350)^3}{K_c} &= 2.0 \\ K_c &= 0.5\times10^{-3}\ \mathrm{W/m-K} \\ K_{\mathrm{Rad}} &= 2.33\times10^{-11}\ \mathrm{W/m-K^4} \end{aligned}\right\} \quad (17)$$

The heat equation provides a direct derivation of the dust layer thickness while adjusting the thermal conductivity for different temperature ranges:

$$Q = -\left(K_c + K_{\mathrm{Rad}}T^3\right)\frac{dT}{da} \quad (18)$$

where Q is heat flow per unit area from the dust surface in watts per meters squared and a is the dust layer thickness in meters. Since Q is constant through the layer at steady state, equation (18) can be integrated as follows:

$$Q\int_0^a da = -\int_{T_1}^{T_2}\left(K_c + K_{\mathrm{Rad}}T^3\right)dT = -\left(K_cT + \frac{K_{\mathrm{Rad}}T^4}{4}\right)\Bigg|_{T_2}^{T_2} \quad (19)$$

Therefore, a becomes simply

$$a = Q^{-1}\left[K_c\left(T_1 - T_2\right) + \frac{K_{\mathrm{Rad}}}{4}\left(T_1^4 - T_2^4\right)\right] \quad (20)$$

For a given set of conditions, the values of Q are established from the Stephan-Boltzmann equation, T_2 is subsequently calculated, and the associated thickness a is determined. A sample calculation is shown for a high-emittance radiator surface (e.g., arc-textured copper, arc-textured niobium, pyrolytic graphite, or carbon-carbon composite) at 800 K with a state-of-the-art emittance of 0.85:

$$Q_1 = \varepsilon_1 k\left(T_1^4 - T_{\mathrm{space}}^4\right) \quad (21)$$

The effective temperature of space from the perspective of a vertical radiator on the Moon may be taken to be in the neighborhood of 222 K, which includes the solar radiation reflected from the Moon and the surface temperature itself, averaged over a lunar cycle. Since the Stephan-Boltzmann constant k is 5.67×10^{-10} W/m^2-K^4,

$$Q_1 = 19\ 624\ \mathrm{W/m^2} \quad (22)$$

If a coverage of lunar dust causes a 25-percent reduction in heat rejected by the radiator, for example, the temperature at the surface of the dust is back-calculated from the same Stephan-Boltzmann relation:

$$0.75Q_1 = \varepsilon_2 k\left(T_2^4 - T_{\mathrm{space}}^4\right) \quad (23)$$

where ε_2 is the emittance of lunar dust. This value, known to be very high, has been measured in the range between 0.9 and 0.95 (Logan et al., 1972), so 0.93 will be used. For this case, the resulting T_2 is 728 K. Equation (18) is then used to predict that a dust layer thickness of 54 μm would cause this 25-percent reduction in performance. Similar calculations were used to obtain the curves in figures 24 and 25, for both the Stirling engine and Brayton cycle systems.

An especially interesting result is produced from these calculations: at very small dust thicknesses, the radiator's performance is actually enhanced by the presence of lunar dust. This might be expected on the basis of our assumption of good thermal contact with the first dust layer and the fact that the emittance of lunar dust exceeds that of the best radiator surfaces. When the dust layer is so thin that the thermal barriers are negligible, this improved radiation works to an advantage. Beyond a certain thickness, however, the poor heat transfer by conduction becomes magnified by many particle interfaces. Therefore, there is no performance penalty for a Brayton cycle radiator unless the dust layer exceeds 11 μm; for a Stirling engine radiator, the threshold is 12 μm. As a point of reference, some parts of the Surveyor III retained as much as 8.7 μm of lunar dust after the sandblasting effects of the Apollo 12 landing (Satkiewicz and Marmo, 1972). It should be noted that in reality a dust layer may include particles from less than 1 μm to 1000 μm, but dust thickness a is meant to represent an average layer thickness.

The assumption that the interface between the radiator surface and the dust particles provides no additional thermal resistance is perhaps optimistic. However, if the radiator surface is roughened, the increased contact area might contribute to enhanced thermal contact. It is possible that the constants K_c and K_{Rad} have subtle variations with temperature which are ancillary to the variation of K_{eff}, but these are not expected to be significant relative to the T^3 contribution. The effective temperature of space T_{space} may actually be lower or higher, depending on the radiator orientation and on the associated view factor to the lunar surface, mountains, the sun, and the Earth; however, it is a secondary effect compared with the T_1^4 term. It is assumed that even a vertical radiator will accumulate lunar dust, as confirmed by the astronaut experiences.

Though these preliminary calculations bear experimental confirmation, they predict a rather serious threat to radiator performance by the presence of lunar dust, particularly in light of the particle fluences estimated in the previous section. The same types of performance degradation can be expected for photovoltaic surfaces as well.

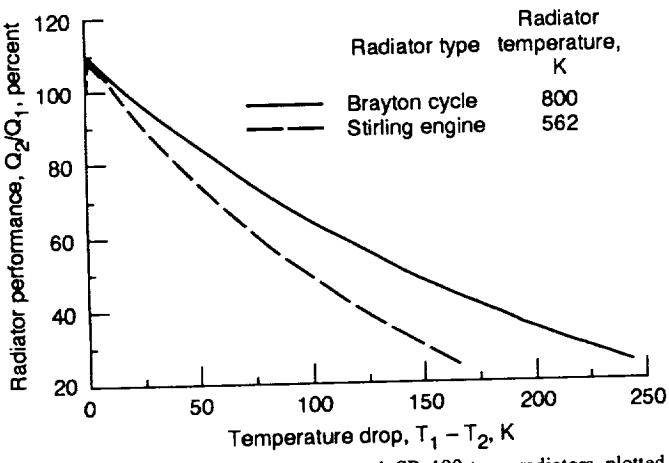

Figure 24.—Performance of dust-covered SP-100-type radiators plotted against the temperature drop across the dust layer. In these calculations, the emittance of the radiator surface, ε_1, is 0.85; the emittance of lunar dust, ε_2, is 0.93; and the effective temperature of space, T_{space}, is 222 K.

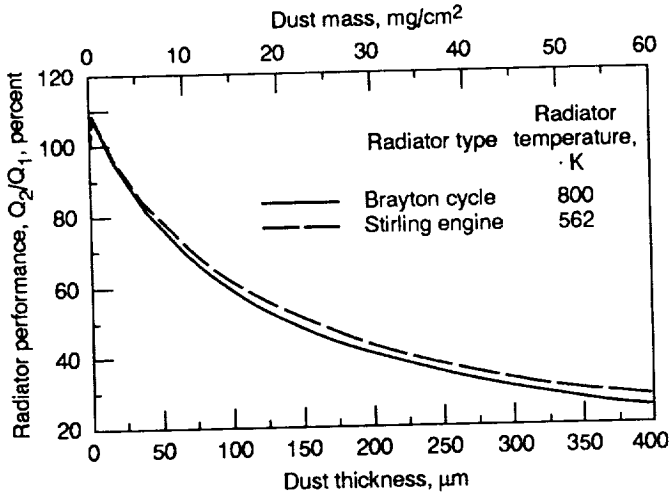

Figure 25.—Performance of dust-covered SP-100-type radiators with varying amounts of lunar dust. In these calculations, the emittance of the radiator surface, ε_1, is 0.85; the emittance of lunar dust, ε_2, is 0.93; and the effective temperatures of space, T_{space}, is 222 K.

Photovoltaic Array Performance

The occlusion of light by a particle layer can be predicted with a simple overlap model. The probability that a single particle will cover a given point on a surface is α/A, where α is the cross-sectional area of the particle and A is the area of the entire surface. Therefore, the probability that the surface is *not* covered by the particle is $(1 - \alpha/A)$. If there are N particles of the same size, each with relative transmittance γ, then the probability of a point on the surface remaining unobscured is $(1 - \gamma\alpha/A)^N$. Now two substitutions are made. First, a dummy variable, j, is defined as

$$j = \frac{A}{\gamma\alpha} \tag{24}$$

Secondly, the mass of all such dust particles M is incorporated into the calculations by its relationship to N through particle volume V and density ρ:

$$N = \frac{M}{V_\rho} = \frac{M}{\rho\left(\frac{\ell bh}{2}\right)} = \frac{2Mj\gamma}{\rho hA} \tag{25}$$

The shape factor in brackets corresponds to particles which are roughly rectangular boxes that were cleaved along the box diagonal, in order to correlate to the preliminary experimental confirmation of the model. In the experiment, 1- by 1-in. glass microscope coverslips were subjected to successive particle dustings and measured for relative transmittance of white light with each dusting. The "dust" selected for these tests was "Minnesota Lunar Simulant-1" (MLS-1), which the University of Minnesota's Space Science Center mines from a quarry in Duluth for its unusually close compositional match to lunar mare soil (Weiblen and Gordon, 1988). After being ground to lunar particle size, many of the MLS-1 particles have the general shape just described; upon sieving, the narrow size fraction used was shown to have an average length of 78 μm, a breadth of 56 μm, and a thickness of approximately 18 μm. The material is assumed to have a density similar to the average lunar particle density: 3.01 g/cm^3 (Duke et al., 1970). The relative transmittance γ of an average particle was estimated to be 0.45 by measuring the relative transmittance of a monolayer of material.

By substitution of N, the fraction of the surface unoccluded by particles of radius R becomes

$$F_{\text{unoccluded}} = F_0\left[\left(1-\frac{1}{j}\right)^j\right]^{2M\gamma/\rho hA} \tag{26}$$

Since A is much larger than α (i.e., j is very large), the bracketed term approaches exp (-1), so the unoccluded area is then

$$F_{\text{unoccluded}} = F_0 \exp\left(\frac{-2M\gamma}{\rho hA}\right) \tag{27}$$

The unoccluded area is directly related to the transmittance of light, to a first approximation. This assumption may slightly underestimate the total light that penetrates a surface by omitting light scattered off particles, but it is expected that back-reflection from the surface itself may offset this factor somewhat. Therefore, the transmission of light through a layer of particles is

$$\tau_2 = \tau_1 \exp\left(\frac{-2M\gamma}{\rho hA}\right) \tag{28}$$

In figure 26 the theoretical model is compared with the experimentally measured values of relative transmittance for different amounts of MLS-1. The agreement is very good, indicating that an exponential relationship well describes the occlusion of light by a coverage of equivalent particles.

Naturally, lunar soil is composed of a complete distribution of particle sizes. Equation (28) can be generalized by taking the product of the probabilities for each possible particle size. This effectively means summing the exponent over all particle sizes and weighting for frequency of occurrence. Subtle manipulation is required to obtain the relative transmittance as a simple function of dust weight for this general case. This is developed in appendix C. However, to summarize, the model was prepared for both spherical and cubic particles. The results are shown in figure 27. The relationship is still an exponential decay of relative transmittance with accumulation. If all lunar particles were spherical (really only true for about 20 percent of lunar soil) a 50-percent reduction would be predicted for 3.5 mg/cm^2 of lunar dust. For particles of higher surface area to volume ratio, the penalty is much greater for the same amount of dust. For example, if all lunar particles were cubic, an accumulation of 3.5 mg/cm^2 would reduce transmittance by 75 percent. As indicated earlier, many lunar particles are vesicular, and therefore the curve for real lunar dust is expected to fall below that for cubic particles.

As a point of reference, it is estimated that 1 mg/cm^2 of lunar soil arrived at the Surveyor III from the landing of the Apollo LM, though some of this was sandblasted away. By this light occlusion model, that amount of dust could reduce transmittance to less than 70 percent. For radiators, this accumulation would enhance performance to 105 percent. Similarly, for a dust layer of 10 mg/cm^2, a radiator would

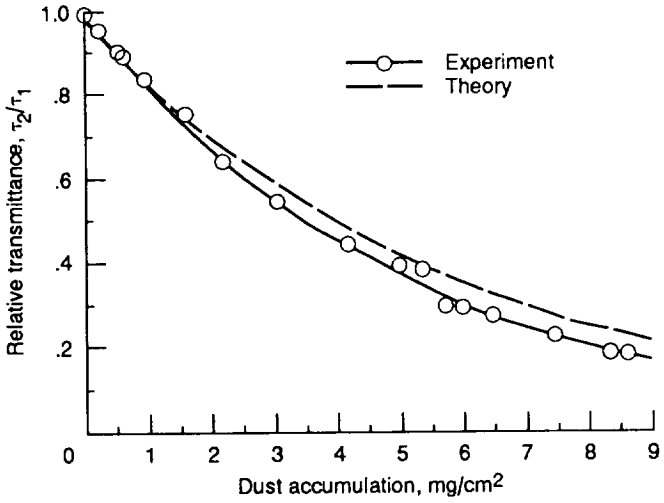

Figure 26.—Transmittance of a glass coverslip with varying amounts of dust. Theory and experiment are compared for a specific particle size and shape. The dust material used is MLS-1, with an average thickness of 18 μm; length, 78 μm; width, 56 μm; relative transmittance, 0.45; and density, 3.0 g/cm^3.

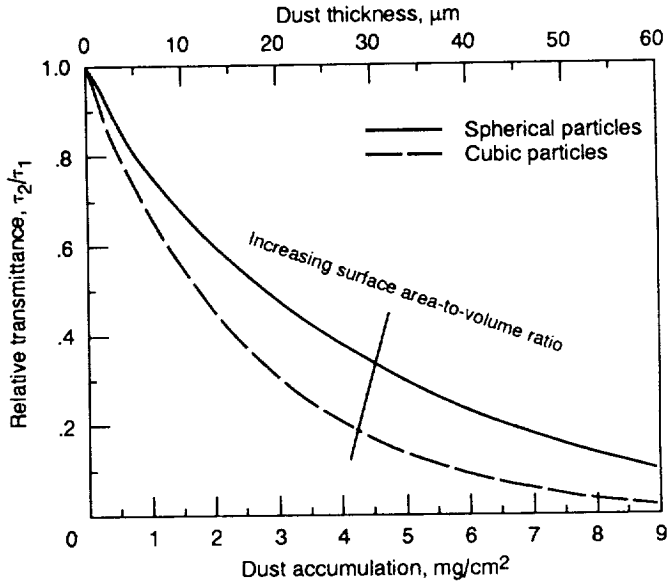

Figure 27.—Predicted transmittance of a glass coverslip with varying amounts of dust. The model has been extended to incorporate the lunar particle size distribution from 1 to 1000 μm. Spherical and cubic particles are compared.

perform at 70 percent efficiency, whereas a solar cell would receive less than 20 percent of its optimal illumination. From these estimates, it can be seen that the penalties for photovoltaics are predicted to be more substantial than those for radiators.

To a first approximation, the relative transmittance of light through a solar cell surface is proportional to relative power output. Therefore, these curves reflect the potentially serious impact of lunar dust on the cell output. Naturally, the optical absorption by the particles varies with wavelength. Similarly, solar cells "respond" to limited bands of the electromagnetic spectrum. Thus a more complete model would show a wavelength dependence. In addition, the inclusion of minor factors, such as light refraction at the surface and diffraction off particles, may help to develop the model.

To obtain a complete assessment of the potential interference of lunar dust with power component performance, it will be necessary to address the many associated factors in further studies. These include analysis of the complex adhesion behavior of lunar particles to power surface materials on the Moon, experimental confirmation of particle trajectories and accumulation, further evaluation of power component performance with lunar dust coverage, and possible techniques to prevent or remove lunar dust from critical surfaces.

Performance Penalties With Time

By invoking the earlier scenario of an O_2/H_2 propulsion excursion vehicle with 26 800-N thrust servicing the lunar base twice a year, one can estimate the performance of dust-covered radiators and photovoltaic arrays as a function of time. The dust accumulations predicted in figure 22 have been combined with the performance decays of radiators

(fig. 25) and photovoltaic arrays (fig. 27) to indicate relationships between performance and distance, and performance and time. In figure 28, model 2 has been developed to show the performance of Stirling engine radiators and photovoltaic arrays as a function of distance from the landing site after 5 yr (10 missions). For both radiators and arrays, the performance is greatly reduced within 500 m of the launchpad, and gradually improves with distance. By 1 km, the predicted penalties for radiators are very small, if it is assumed that no thermal barrier exists between the dust layer and the radiator. For photovoltaic arrays, the dust accumulation from 10 lunar missions can be expected to reduce performance to roughly 40 percent at 1 km and 90 percent at 2 km.

Figure 29 shows the progressive degradation in Stirling engine radiator performance over time for various distances, as derived from model 2. As discussed previously, when the accumulation is less than 11-μm thick, the theoretical performance is enhanced by the high emittance of lunar soil. For radiators within 1 km, however, the dust accumulation resulting from 10 surface missions is sufficient to inhibit heat rejection and degrade performance.

The comparable plot of photovoltaic array performance with time is shown in figure 30. Arrays located within 1 km of the landing site, in particular, experience rapid deterioration in performance in 5 yr. An array at 500 m will be reduced to 85 percent of original performance after 3 mo; at 1 km and 1.5 km, performance will degrade to 85 percent by 1 yr and 2.5 yr, respectively. From these projections it is clear that dust from lunar excursion vehicles alone constitutes an enormous threat to power system components. Additional dust suspended by rovers and mining and construction operations will significantly magnify the predicted degradation. Furthermore, although inconsequential individually, the accumulations resulting from primary and secondary meteoroid impacts, electrostatic levitation at the terminator, and human activities on foot will also contribute to the net deterioration of component performance.

Implications and Alternatives

The most obvious way to reduce lunar dust accumulation might be to position power components as far away as possible from the center of base activity. The reduced exposure to dust must be balanced against the penalties of cabling power great distances. At best, the resulting compromise will still leave power components vulnerable to a number of dust sources unless additional measures are incorporated.

Unfortunately, evidence indicates that lunar dust adheres readily to a variety of surfaces. Mechanical removal techniques would be astronaut-intensive and logistically very difficult because of the large surface areas necessarily involved. Restoring surfaces to original clean condition is not likely, and removal processes could abrade the surfaces. For these reasons, removal would be performed only rarely, and yet it

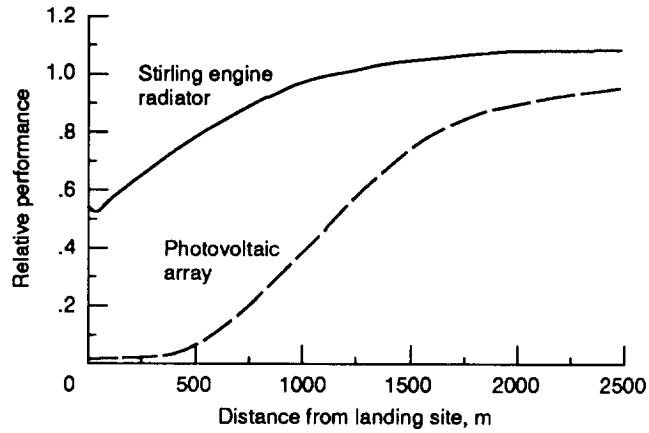

Figure 28.—Predicted radiator and photovoltaic array performance with distance from landing site after 5 yr (10 missions) of a 26 800-N excursion vehicle. It was assumed that the dust profile produced by launch is equivalent to that from landing, and that thrust is proportional to distance and to the square root of particle flux. Data was derived from model 2.

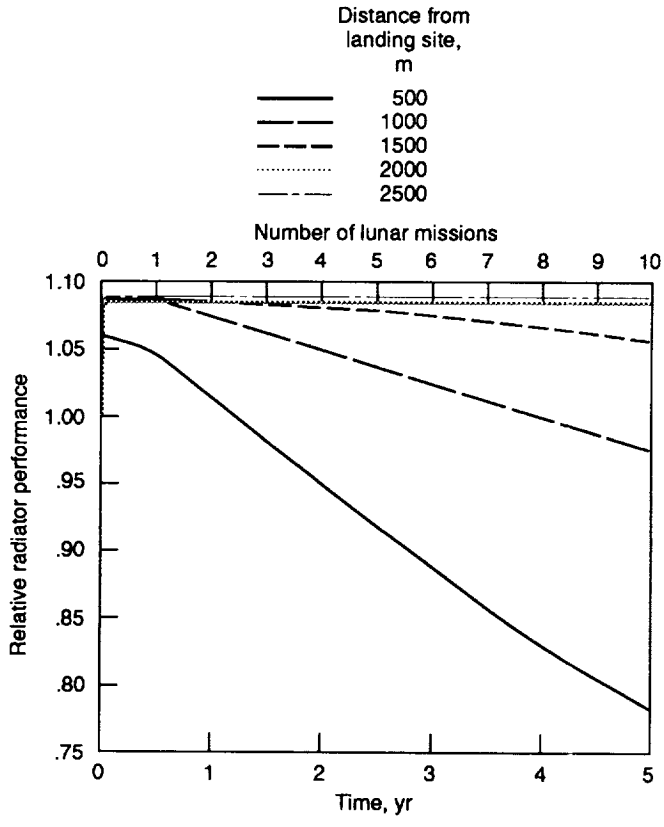

Figure 29.—Predicted Stirling engine radiator performance after the accumulation of lunar dust resulting from the launch and landing of 26 800-N lunar excursion vehicles. This projection, derived from model 2, compares radiator performance as a function of time for different distances from the landing site. Notice that small accumulations actually enhance performance, providing that the dust/radiator interface is not a thermal barrier.

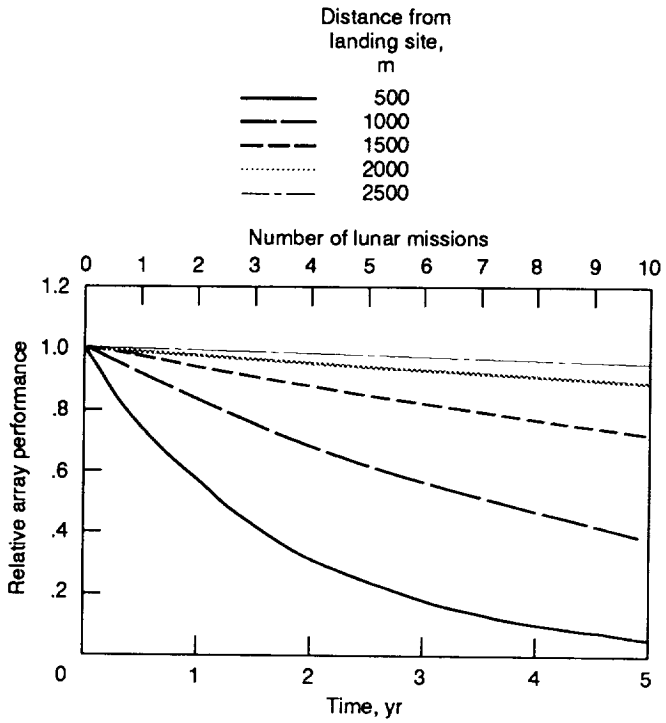

Figure 30.—Predicted photovoltaic array performance after the accumulation of dust resulting from the launch and landing of 26 800-N lunar excursion vehicles. This projection, derived from model 2, compares array performance as a function of time for different distances from the landing site.

is likely to be unacceptable to allow surfaces to acquire dust accumulations that would periodically reduce performance. Consequently, the solution to lunar dust accumulation on sensitive surfaces becomes one of prevention rather than removal.

Therefore, a defensive position is recommended against dust accumulation. First, where possible, dust suspension should be reduced to a minimum. In some cases this could be accomplished by simple measures, such as improved fenders for surface roving vehicles, more flexible spacesuits, or restricted access to sensitive areas. On a grander scale, base layout could be designed specifically to reduce dust suspension, separating power components as far as possible from rocket activity, perhaps using natural landspace features for protection. Launchpads might be glazed, and tracks or compacted roads could be constructed for regular traffic routes. It could be helpful to lay platforms in access areas and to separate lunar ores from regolith material *in situ* so that minimal amounts of soil are transported to the central base area. Unfortunately, this degree of defense may require more resources and manpower—both in the design stages and in actual base construction—than is available.

For dust that is inevitably suspended despite all measures, an extra defensive strategy may be necessary. Protective mechanical barriers or dust screens might be used to prevent penetration into the vicinity of sensitive equipment. Such screens could be activated by a signal from a flag made of a piezoelectric film, like polyvinylidene difluoride (J. Graf, 1990, NASA Johnson Space Center, Houston, TX, personal communication; and Amato, 1989). When the dust subsides, the screens could be withdrawn. Lunar particles may be triboelectrically charged during disturbances like rocket blasts, and therefore an electrostatic fence might be a method for diverting these particles from photovoltaic arrays or radiators. A high voltage, alternating potential could prevent dust buildup on the fence itself, while deflecting both positively and negatively charged particles. Preliminary laboratory studies will help to establish the charge of disturbed lunar particles as well as the motion of these particles under the influence of an electric field in vacuum.

Summary of Results

The Moon is a hazardous place for surfaces sensitive to dust accumulation. The transport of large amounts of lunar dust can be expected. Aside from natural sources of suspended dust, several forms of human activity on a lunar base, including walking, operating surface vehicles, mining and construction, and most importantly, rocket launch and landing, will disturb significant amounts of dust. Components returned from the Surveyor III proved that significant accumulation had occurred at a distance of 155 m from an Apollo lunar landing. From shadowing and pitting, the average particle velocity was estimated to be between 40 and 100 m/s, arriving at an angle of almost 0° during touchdown. From this evidence, the overall particle velocity distribution was modeled for three cases, and accumulation distributions were subsequently derived. These distributions predict that surfaces will acquire substantial accumulations of lunar dust from a lunar module-type descent engine even up to distances of 2 km. Future lunar excursion vehicles that would service a permanent base are likely to require higher thrust levels and to descend and ascend frequently. As an example, the dust accumulation distribution resulting from the launch and landing of a 26 800-N vehicle has been predicted as a function of time and distance from the landing site. With the additional contributions of other human activities, lunar dust accumulation on sensitive surfaces is likely to be an enormous problem—particularly for power system components. Therefore, the use of photovoltaic arrays and radiators will be successful provided lunar dust effects are considered in their design and use. Otherwise, the performance penalties could be severe.

Two models were developed to estimate the associated performance reduction of radiator surfaces and photovoltaic arrays. Both predict exponential decay with increasing accumulation. For radiators, very thin dust layers may actually enhance performance because of the high emissivity of lunar dust if the first layer is in intimate thermal contact with the radiator. A layer of more than about 11 μm would limit the ejection of heat because the thermal conductivity of lunar soil is extremely poor. The model for photovoltaic arrays estimates

the reduction in relative power output by calculating the relative light transmittance through a dust layer. The general exponential relationship between transmittance and dust accumulation was confirmed by preliminary experimental measurements. The penalties for both photovoltaic and radiator surfaces are significant from dust accumulations that can be reasonably expected from normal lunar base activities. Lunar particle adhesive forces are reported to be so strong that dust removal techniques are likely to be unsuccessful. Therefore, a defensive position against accumulation is recommended. Such an approach might include barriers, electrostatic particle fences, glazed launchpads, compacted roads, and improved vehicle fenders in addition to strategic placement of power components on a lunar base.

Acknowledgments

The authors wish to gratefully acknowledge Curtis Stidham, Sverdrup Technology, Inc., and Bruce Banks, NASA Lewis Research Center, for their insight into lunar rover particle ejection and many other useful discussions. The authors also thank Robert Siegel, NASA Lewis Research Center, for his helpful guidance in heat transfer calculations.

Lewis Research Center
National Aeronautics and Space Administration
Cleveland, Ohio, May 30, 1991

Appendix A
Symbols

A	area of a surface, cm^2
a	dust layer thickness, m
b	particle breadth, μm
C, C', C_1, C_2	constants
D	diameter of a spherical particle, μm
D_1, D_2	diameters of two hypothetical spherical particles
$F_{unoccluded}$	area fraction of a surface not occluded by particles
F_0	original area fraction of a surface
g	lunar surface gravitation
h	particle height, mm
h_s	height of a spherical segment of one base, m
j	dummy variable
j_n	dummy variable specific to a particle of size n
K_c	thermal conductivity, W/m-K
K_{eff}	effective thermal conductivity (sum of components of radiation and conduction, $W/m\text{-}K^4$)
K_{Rad}	thermal radiation
k	Stephan-Boltzmann constant, 5.67×10^{-8} $W/m^2\text{-}K^4$
ℓ	particle length, μm
M	total mass of particles of a specific size, mg
M_{dist}	mass of a complete distribution of lunar particle sizes, mg/dist
M_{tot}	total mass of particles of many sizes, mg
m	particle mass, mg
m_{ave}	average mass of a lunar particle, g
m(D)	mass of a particle of diameter D, mg
m_n	mass of a particle of size n, mg
N	number of particles
N_n	number of particles of size n
$N(D)$	number of spherical particles of diameter D
$N(m)$	number of spherical particles of mass m
$N(R_n)$	lunar particle size distribution j number of lunar particles of a given radius R_n.
$N(v)$	number of particles with velocity v_0
$N(x)$	number of particles accumulated as a function of x
$N(\Theta)$	number of particles accumulated as a function of Θ
n	designation given to a specific particle size
P	cumulative mass percentage of particles of size D or smaller
P_1, P_2	cumulative mass percentages of particles less than or equal to hypothetical particles of diameters D_1 and D_2
Q	heat flow per unit area, W/m^2
Q_1	heat flow per unit area from a clean radiator, W/m^2
Q_2	heat flow per unit area from a dust-covered radiator surface, W/m^2
R	particle radius, μm
R_n	radius of a particle of size n, μm
r	radius of a sphere, m
S, S'	constants
T	temperature, K

T_{space}	average effective temperature of space for a vertical radiator on the lunar surface aligned with the lunar ecliptic
T_1	temperature at the surface of a clean radiator, K
T_2	temperature at the surface of a dust layer on a radiator, K
t	time, s
V	volume of a particle, μm^3
V_n	volume of a particle of size n, μm^3
V_{ss}	volume of a spherical segment of one base, m^3
v_{rot}	component of a particle's velocity vector associated with a rover wheel's rotation, m/s
v_{rover}	lunar roving vehicle's velocity vector, m/s
v_{total}	total velocity vector of a particle ejected from a rover wheel, m/s
v_{trans}	component of a particle's velocity vector associated with the translational motion of a rover wheel, m/s
v_0	initial particle velocity, m/s
v_{0y}	initial particle velocity in the vertical direction, m/s
$v_y(t)$	particle velocity in the vertical direction as a function of time
x	horizontal distance traveled by a particle ejected by a lunar rover wheel, m
$\hat{x}$	unit vector in the x direction
y	vertical position in a particle trajectory, m; unit vector in the y direction
y_{max}	maximum height of particle trajectory, m
z_n	diagonal of a cubic particle of size n, μm
α	cross-sectional area of a particle, cm^2
α_n	cross-sectional area of a particle of size n, cm^2
β	mean velocity in normal-type velocity distribution, m/s
γ	relative transmittance of a lunar particle
ε_1	emittance of a radiator surface
ε_2	emittance of lunar dust
Θ	rover wheel angle defining the point of particle ejection
ρ	material density of a particle, g/cm^3
σ	standard deviation in normal-type velocity distribution, m/s
τ_1	optical transmittance of a clean surface
τ_2	optical transmittance of a dust-covered surface
ϕ	particle ejection angle

Appendix B
Lunar Particle Size Distribution

The data available about the particle size distribution of lunar soil is always presented as a "cumulative weight percentage distribution" — that is, as "percent finer by weight" as a function of particle size. This is directly related to the method by which the distribution is measured: a known amount of lunar soil is sieved through a succession of meshes with smaller and smaller openings. The total weight (these authors prefer to use "mass") of material that passes through a screen is plotted against that size opening. Considering the intricacies of handling and weighing minute quantities of particles, different laboratories show general agreement for similar soils. Consistently, the entire distribution lies between 1 mm and roughly 1 μm. The cumulative mass percentage of particles is fairly logarithmically linear with particle size. The negative slope indicates that the soil is heavily skewed toward finer size fractions.

Occasionally it is more useful to have a particle size distribution in the form "number of particles" versus particle size or particle mass. This distribution can be achieved through manipulation of the cumulative percentage distribution. Consider figure 31—for every size interval ΔD, the corresponding ΔP is defined as P_1 (the percent of particles of mass less than that associated with D_1), subtracted from P_2 (the percent of particles of mass less than that associated with D_2), which yields ΔP (the total mass percent falling between D_1 and D_2). In the limit as $\Delta D \rightarrow 0$, the mass percent of all particles of size D is dP/dD evaluated at D. Since the absolute mass of particles only differs from the mass percent of particles of size D by the constant "total mass/100," we can treat dP/dD as the absolute mass of particles. For a general particle size D,

$$\frac{dP}{dD} = N(D)[m(D)] \qquad \text{(B1)}$$

where $m(D)$ is the mass per particle of size D, and $N(D)$ is the number of particles of size D, which we are trying to establish. Mass is generally related to the cube of particle size—the constants associated with density and shape can be ignored for the time being. Therefore,

$$N(D) = \left(\frac{1}{D^3}\right)\frac{dP}{dD} \qquad \text{(B2)}$$

Since the distribution P is logarithmic in D, $dP/dD \propto 1/D$. Therefore, the number of particles of a given size becomes

$$N(D) \propto \frac{1}{D^4} \qquad \text{(B3)}$$

Any neglected constants are automatically accounted for by normalizing the distribution function over all particles, from 1 to 1000 μm:

$$1 = C_1 \int_{1\,\mu m}^{1000\,\mu m} \frac{1}{D^4}\,dD = \frac{-C_1 D^{-3}}{3}\Bigg|_{1\,\mu m}^{1000\,\mu m} = \frac{C_1}{3}$$

$$\text{for } C_1 = 3 \qquad \text{(B4)}$$

So finally,

$$N(D) = \frac{3}{D^4} \qquad \text{(B5)}$$

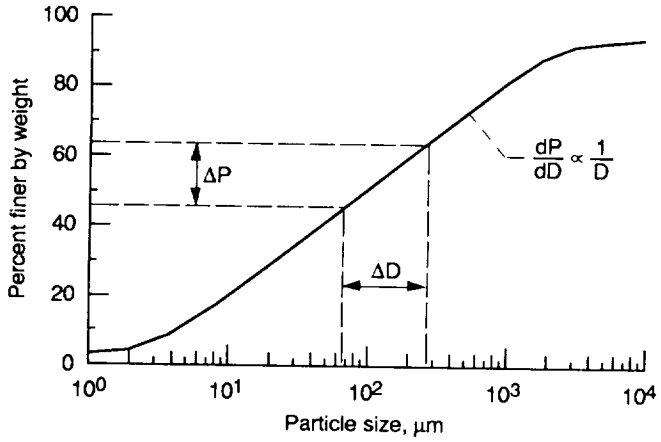

Figure 31.—Example of a cumulative mass percentage distribution; the standard format of a lunar particle size distribution.

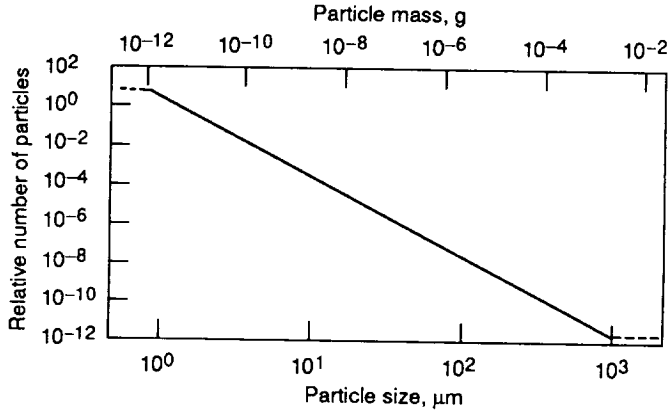

Figure 32.—Lunar particle size distribution, derived from a cumulative weight percentage distribution and normalized from 1 to 1000 μm to show relative number of particles of a given size.

gives the relative number of particles for a given size D. This is shown in figure 32.

The distribution can also be written as a function of particle mass $N(m)$, using the relation

$$D \propto m^{1/3} \tag{B6}$$

$$N(m) = m^{-4/3} \tag{B7}$$

Again this is easily normalized. Assuming spherical particles of material density 3 g/cm^3, the limits of integration become 1.57×10^{-12} g (1-μm particles) and 1.57×10^{-3} g (1-mm particles).

$$\left.\begin{aligned} 1 = C_2 \int_{157\times10^{-12}\ \mathrm{g}}^{157\times10^{-3}\ \mathrm{g}} m^{-4/3}\,dm = -3\left(m^{-1/3}\right)\Big|_{1.57\times10^{12}\ \mathrm{g}}^{1.57\times10^{-3}\ \mathrm{g}} \\ C_2 = 1.16\times10^{-4} \end{aligned}\right\} \tag{B8}$$

$$N(m) = 1.16\times10^{-4}\left(m^{-4/3}\right) \tag{B9}$$

This is also shown in figure 32.

As a final note it should be mentioned that although particles smaller than 1 μm are normally off the end of cumulative particle size distributions (and are, therefore, not included in these modified distributions), their numbers may actually be significant. In fact, large numbers of submicrometer particles have been observed in many microscopic investigations. The inconsistency occurs because the finest particles adhere very tenaciously to larger particles, both because of the frictional electrostatics created by sieve shakers and because of laboratory moisture. Consequently, these fine particles do not penetrate the screens despite their size. Unfortunately this size fraction of unestablished population may represent those particles most readily transported and accumulated on vulnerable power surfaces.

Appendix C
Modeling Relative Transmittance of a Dust-Covered Surface for Particles of Different Sizes and Shapes

The general model for the relative transmittance of a surface with a given weight of dust is developed in much the same way as for the specific case in which only one particle size is present. Now, however, the probability terms for all possible sizes are multiplied together:

$$\frac{\tau_2}{\tau_1} = \left(1-\frac{\alpha_1}{A}\right)^{N_1}\left(1-\frac{\alpha_2}{A}\right)^{N_2}\cdots\left(1-\frac{\alpha_n}{A}\right)^{N_n} \qquad \text{(C1)}$$

Each term corresponds to the probability that a particle with cross-sectional area α_n, does not cover an imaginary point on the total surface A. Then N_n is the number of particles of size n. If the particles are spherical, then

$$N_n = \frac{m_n}{V_n\rho} = \frac{m_n}{\frac{4}{3}\pi R_n^3\rho} = \frac{3m_nA}{4\pi R_n^2R_n\rho A} = \frac{3m_nj_n\gamma}{4R_n\rho A} \qquad \text{(C2)}$$

where M_n is the total weight of all particles of size n, V_n is the volume of a particle of size n, ρ is a particle's density, and the dummy variable j_n is $\gamma A/\alpha_n$, as before. The relative transmittance then becomes

$$\frac{\tau_2}{\tau_1} = \left[\left(1-\frac{1}{j_1}\right)^{j_1}\right]^{\frac{3m_1\gamma}{4R_1\rho A}}\left[\left(1-\frac{1}{j_2}\right)^{j_2}\right]^{\frac{3m_2\gamma}{4R_2\rho A}} \cdots \left[\left(1-\frac{1}{j_n}\right)^{j_n}\right]^{\frac{3m_n\gamma}{4R_n\rho A}} \qquad \text{(C3)}$$

Each bracketed term equals exp (-1) by the following:

$$\lim_{j_n\to\infty}\left[\left(1-\frac{1}{j_n}\right)^{j_n}\right]^{\alpha} = \exp(-\alpha) \qquad \text{(C4)}$$

Recall, $A>>\alpha_n$, and so j is large. Therefore, the relative transmittance simplifies to

$$\frac{\tau_2}{\tau_1} = \exp\left[\frac{-3\gamma}{4\rho A}\left(\frac{m_1}{R_1}+\frac{m_2}{R_2}+\cdots+\frac{m_n}{R_n}\right)\right] \qquad \text{(C5)}$$

In order to proceed further, a more useful form of m_n is necessary, in terms of the measurable value M_{tot}, the total mass of dust:

$$m_n = \left[N(R_n)\frac{M_{tot}}{M_{dist}}\right]V_n\rho \qquad \text{(C6)}$$

In this equation, the bracketed term is the number of particles of a given size n. The function $N(R_n)$ may be recognized as the distribution function of lunar soil normalized for all radii from 0.5 to 500 μm. The parameter M_{dist} is the effective mass of one complete distribution of lunar soil, related to $N(R)$ as follows:

$$\begin{aligned} M_{dist} &= \int_{\text{all } R} N(R)V_n\rho dR \\ &= \int_{0.5\mu m}^{500\mu m}\left[\frac{3}{(2R)^4}\right]\frac{4}{3}\pi R^3\left(3\times10^{-9}\,\frac{\mu g}{\mu g^3}\right)dR \\ &= \frac{\pi}{4}\left(3\times10^{-9}\right)\left(ln\,500 - ln\,0.5\right) \\ &= 1.63\times10^{-8}\ \mu g/dist \end{aligned} \qquad \text{(C7)}$$

Combining all the constants in equation (C5) as S yields a relative transmittance of

$$\frac{\tau_2}{\tau_1} = \exp\left\{\frac{-3\gamma}{4\rho A}(M_{tot})S\left[N(R_1)\frac{R_1^3}{R_1}+N(R_2)\frac{R_2^3}{R_2}+\cdots+N(R_n)\frac{R_n^3}{R_n}\right]\right\} \qquad \text{(C8)}$$

The solution to the series of terms in brackets in equation (C8) is found by integrating for all R

$$\frac{\tau_2}{\tau_1} = \exp\left[\frac{-3\gamma}{4\rho A}(M_{tot})\ S\int_{\text{all } R}N(R)R^2dR\right]$$

$$= \exp\left[\frac{-3\gamma}{4\rho A}(M_{tot})\, S \int_{0.5\,\mu m}^{500\,\mu m} \frac{3}{(2R)^4} R^2\, dR\right]$$

$$= \exp\left[\frac{-3\gamma}{4\rho A}(M_{tot})\, S\, \frac{3}{16}\left(\frac{-1}{R}\right)\Bigg|_{0.5\,\mu m}^{500\,\mu m}\right] \qquad \text{(C9)}$$

The values for γ and ρ, 0.45 and 3.0 g/cm^3, respectively, are substituted; and units are adjusted to give the predicted relative transmittance for spherical particles:

$$\frac{\tau_2}{\tau_1} = \exp\left(-0.0325 \frac{M_{tot}}{A}\right) \qquad \text{(C10)}$$

where M_{tot}/A can be measured experimentally in mg/cm^2.

Similarly, a model is developed for cubic particles of the same size distribution. For this case, particle length z_n corresponds to the cube diagonal. Because of the different shape factor, equation (C4) looks like

$$\frac{\tau_2}{\tau_1} = \exp\left[\frac{-\sqrt{3}\gamma}{\rho A}\left(\frac{m_1}{z_1} + \frac{m_2}{z_2} + \cdots + \frac{m_n}{z_n}\right)\right] \qquad \text{(C11)}$$

and M_{dist} equals 1.196×10^{-8} mg/distribution. Equation (C7) takes the form

$$\frac{\tau_2}{\tau_1} = \exp\left\{\frac{-\sqrt{3}\gamma}{\rho A}(M_{tot})S' \times \left[N(z_1)\frac{z_1^3}{z_1} + N(z_2)\frac{z_2^3}{z_2} + \cdots + N(z_n)\frac{z_n^3}{z_n}\right]\right\} \qquad \text{(C12)}$$

Integrating over all z, yields

$$\frac{\tau_2}{\tau_1} = \exp\left[\frac{-\sqrt{3}\gamma}{\rho A}\left(M_{tot}\right) S' \int_{1\,\mu m}^{1000\,\mu m} \frac{3}{z^2} dz\right] = \exp\left(-0.0584 \frac{M_{tot}}{A}\right) \qquad \text{(C13)}$$

The curves for the spherical and cubic particle models are shown in figure 25.

References

Allen, L.H.: The Lunar Sunset Phenomenon. Surveyor: Program Results, NASA SP-184, 1969, pp. 413-418.

Amato, I.: Fantastic Plastic. Science News, vol. 136, no. 21, Nov. 18, 1989, pp. 328-329.

Anderson, D.L., et al.: Particle Impact and Optical Property Analysis of the Surfaces of Surveyor 3 Materials. Analysis of Surveyor 3 Material and Photographs Returned by Apollo 12, NASA SP-284, 1972, pp. 76-88.

Apollo 12 Technical Crew Debriefings (U), Dec. 1, 1969, Manned Spacecraft Center, Houston TX.

Baker, D.: Lunar Roving Vehicle: Design Report. Spaceflight, vol. 13, no. 7, July 1971, pp. 234-240.

Banks, B.A., et al: Arc-Textured Metal Surfaces for High Thermal Emittance Space Radiators. NASA TM-100894, 1988.

Brownlee, D.E.; Bucher, W.; and Hodge, P.: Primary and Secondary Micrometeoroid Impact Rate on the Lunar Surface; A Direct Measurement. Analysis of Surveyor 3 Material and Photographs Returned by Apollo 12, NASA SP-284, 1972, pp. 143-151.

Carrier, D.: Geotechnical Considerations. The Lunar Source Book, G.H. Heiken, D.T. Vaniman, and B.M. French, eds., Cambridge University Press, Chap. 7.2, 1991.

Carroll , W.F.; and Blair, Jr., P.M.: Lunar Dust and Radiation Darkening of Surveyor 3 Surfaces. Analysis of Surveyor 3 Material and Photographs Returned by Apollo 12, NASA SP-284, 1972, pp. 23-28.

Carroll, W.F., et al.: Returned Surveyor 3 Hardware: Engineering Results. Analysis of Surveyor 3 Material and Photographs Returned by Apollo 12, NASA SP-284, 1972a, pp. 15-21.

Carroll, W.F., et al: Introduction. Analysis of Surveyor III Material and Photographs Returned by Apollo 12, NASA SP-284, 1972b, pp. 1-8.

Cour-Palais, B.G., et al.: Results of Examination of the Returned Surveyor 3 Samples for Particulate Impacts. Analysis of Surveyor 3 Material and Photographs Returned by Apollo 12, NASA SP-284, 1972, pp. 158-167.

Cremers, C.J.; and Birkebak, R.C.: Thermal Conductivity of Fines From Apollo 12. Proc. 2nd Lunar Science Conference, Vol. 3, MIT Press, 1971, pp. 2311-2315.

Criswell, D.R.: Horizon-Glow and the Motion of Lunar Dust. Photon and Particle Interactions With Surfaces in Space, R.J.L. Grard, ed., D. Reidel Pub. Co., Dordrecht-Holland, 1973, pp. 545-556.

Duke, M.B., et al.: Lunar Soil: Size Distribution and Mineralogical Constituents. Science, vol. 167, Jan. 30, 1970, pp. 648-650.

Hammock, W.R., Jr., Currie, E.C.; and Fisher, A.E.: Apollo Experience Report—Descent Propulsion System. NASA TN D-7143, 1973.

Humphries, C.E.; and Taylor, R.E.: Apollo Experience Report—Ascent Propulsion System. NASA TN D-7082, 1973.

Inculet, I.I.; and Criswell, D.R.: Electrostatic Beneficiation of Ores on the Moon Surface. Electrostatics 1979, J. Lowell, ed., Institute of Physics, Bristol, England, 1979, pp. 45-53.

Jaffe, L.D.: Blowing of Lunar Soil by Apollo 12: Surveyor 3 Evidence. Analysis of Surveyor 3 Material and Photographs Returned by Apollo 12, NASA SP-284, 1972, pp. 94-96.

Jaffe, L.D., et al: Principal Scientific Results From the Surveyor Program. Surveyor: Program Results. NASA SP-184, 1969, pp. 13-17 (Also, Icarus, vol. 12, pp. 156-160).

Jaffe, L.D.; and Steinbacher, R.H.: Introduction. Surveyor: Program Results. NASA SP-184, 1969, pp. 1-12.

Keihm, S.J.; and Langseth, M.G., Jr.: Surface Brightness Temperatures at the Apollo 17 Heat Flow Site: Thermal Conductivity of the Upper 15 cm of Regolith. Proc. 4th Lunar Science Conference, W.A. Gose, ed., Pergamon Press, 1973, Vol. 3, pp. 2503-2513. (Also, Geochim. Cosmochim. Acta, Suppl. 4).

Langseth, M.G., Jr.; Keihm, S.J.; and Chute, J.L., Jr.: Heat Flow Experiment. Apollo 17 Preliminary Science Report, NASA SP-330, 1974, pp. 9-1 to 9-24.

Logan, L.M., et al.: Midinfrared Emission Spectra of Apollo 14 and 15 Soils and Remote Compositional Mapping of the Moon. Proc. 3rd Lunar Science Conference., Vol. 3, D.R. Criswell, ed., MIT Press, 1972, pp. 3069-3076. (Also, Geochim. Cosmochim. Acta, Suppl. 3).

Lunar Base Launch and Landing Facility Conceptual Design. (EEI-88-178, Eagle Engineering Inc.; NASA Contract NAS9-17878), NASA CR-172049, 1988.

McKay, D.S.; Fruland, R.M.; and Heiken, G.H.: Grain Size and the Evolution of Lunar Soils. Proc. 5th Lunar Science Conference, Vol. 1, W.A Gose, ed., Pergamon Press, 1974, pp. 887-906.

Milwitzky, B.: Preface. Surveyor Program Results, NASA SP-184, 1969, pp. v-vii.

Milwitzky, B., and Dwornik, S.E.: Introduction. Surveyor III: A Preliminary Report, NASA SP-146, 1967, pp. 3-7.

Mitchell, J.K., et al.: Soil Mechanics Experiment. Apollo 14 Preliminary Science Report, NASA SP-272, 1971, pp. 87-108.

Morris, O.: Apollo 17 Mission Report. NASA TM X-69292, JSC-07904, 1973.

Morris, R.V., et al.: Handbook of Lunar Soils, Part I: Apollo 11-15, and Part II: Apollo 16-17. JSC-19069, NASA Johnson Space Center, July 1983.

Mullis, C.H.: A Study and Analysis of the MSFC Lunar Roving Vehicle Dust Profile Test Program. NASA CR-121075, 1971.

Nickle, N.L.: Dynamic Considerations of Dust on the Television Camera Mirror. Analysis of Surveyor 3 Material and Photographs Returned by Apollo 12, NASA SP-284, 1972, pp. 51-59.

Nickel, N.L., and Carroll, W.F.: Summary and Conclusions. Analysis of Surveyor III Material and Photographs Returned by Apollo 12, NASA SP-284, 1972, pp. 9-13.

Papike, J.J.; Simon, S.B.; and Laul, J.C.: The Lunar Regolith: Chemistry, Mineralogy, and Petrology. Rev. Geophys. Space Phys., vol. 20, no. 4, Nov. 1982, pp. 761-826.

Pelizzari, M.A.; and Criswell, D.R.: Lunar Dust Transport by Photoelectric Charging at Sunset. Proc. 9th Lunar Planetary Science Conference, Vol. 3, R.B. Merrill, ed., Pergamon, 1978, pp. 3225-3227.

Phillips, P.G.; Simonds, C.H.; and Stump, W.R.: Lunar Base Launch and Landing Facilities Conceptual Design. Lunar Bases & Space Activities in the 21st Century, Apr. 1988, Houston, TX, Paper No. LBS-88-196.

Rennilson, J.J.; and Criswell, D.R.: Surveyor Observations of Lunar Horizon-Glow. The Moon, Vol. 10, June 1974, pp. 121-142.

Rennilson, J.; Holt, H.; and Moll, K.: Changes in Optical Properties of the Surveyor 3 Camera, Analysis of Surveyor 3 Material and Photographs Returned by Apollo 12, NASA SP-284, 1972, pp. 60-76.

Rhee, J.W.; Berg, O.E.; and Wolf, H.: Electrostatic Dust Transport and Apollo 17 LEAM Experiment. COSPAR Space Research, Vol. 17, Pergamon Press, 1977, pp. 627-629.

Satkiewicz, F.G.; and Marmo, F.F.: Sputter-Ion Source Mass Spectrometer Analysis of Samples Cut From the Surveyor 3 Camera. Analysis of Surveyor 3 Material and Photographs Returned by Apollo 12, NASA SP-284, 1972, pp. 91-94.

Scott, R.F., et al.: Preliminary Geologic Investigation of the Apollo 12 Landing Site: Mechanical Properties of the Lunar Regolith. Apollo 12 Preliminary Science Report, NASA SP-235, 1970, pp. 161-182.

Scott, R.F.; Roberson, F.I.; and Clary, M.C.: Soil Mechanics Surface Sampler: Lunar Surface Tests and Results, Surveyor III: A Preliminary Report, NASA SP-146, 1967, pp. 61-93.

Smith, R.E., and West, G.S., compilers: Space and Planetary Environment Criteria Guidelines for Use in Space Vehicle Development, Vol. I, 1982 Revision, NASA TM-82478, 1983.

Strangway, D.W.: Moon: Electrical Properties of the Uppermost Layers. Science, vol. 165, Sept. 5, 1969, pp. 1012-1013.

Taylor, S.R.: Lunar Science: A Post-Apollo View. Pergamon Press, New York, 1975.

Weiblen, P.W.; and Gordon, K.L.: Characteristics of a Simulant for Lunar Surface Materials. Lunar Bases & Space Activities in the 21st Century, April 1988, Houston TX, Paper No. LBS-88-213.

West, G.S. Jr.; Wright; J.J.; and Euler, H.C., eds.: Space and Planetary Criteria Guidelines for Use in Space Vehicle Development. NASA TM-78119-REV., 1977.

Zook, H.A., et al.: The Interplanetary Micrometeoroid Flux and Lunar Primary and Secondary Microcraters. Properties and Interactions of Interplanetary Dust, R.H. Giese and P. Lamy, eds., D. Reidel Pub. Co., Dordrecht-Holland, 1985, pp. 89-96.

Zook, H.A., et al.: Lunar Primary and Secondary Microcraters and the Micrometeoroid Flux. 15th Lunar and Planetary Science Conference, 1984, pp. 965-966.

REPORT DOCUMENTATION PAGE

Form Approved
OMB No. 0704-0188

1. AGENCY USE ONLY (*Leave blank*)	2. REPORT DATE	3. REPORT TYPE AND DATES COVERED
	November 1991	Final Contractor Report

4. TITLE AND SUBTITLE
Lunar Dust Transport and Potential Interactions With Power System Components

5. FUNDING NUMBERS
WU 506-41-41
C NAS3-25266

6. AUTHOR(S)
Cynthia M. Katzan and Jonathan L. Edwards

7. PERFORMING ORGANIZATION NAME(S) AND ADDRESS(ES)
Sverdrup Technology, Inc.
Lewis Research Center Group
2001 Aerospace Parkway
Brook Park, Ohio 44142

8. PERFORMING ORGANIZATION REPORT NUMBER
E-6145

9. SPONSORING/MONITORING AGENCY NAMES(S) AND ADDRESS(ES)
National Aeronautics and Space Administration
Lewis Research Center
Cleveland, Ohio 44135-3191

10. SPONSORING/MONITORING AGENCY REPORT NUMBER
NASA CR-4404

11. SUPPLEMENTARY NOTES
Project Manager, Bruce Banks, Power Technology Division, NASA Lewis Research Center. Cynthia M. Katzan, Sverdrup Technology, Inc., Lewis Research Center Group, 2001 Aerospace Parkway, Brook Park, Ohio 44142; Jonathan L. Edwards, Marshall University, Huntington, West Virginia 25701 and Summer Student Intern at NASA Lewis sponsored by Case Western Reserve University. Responsible person, Cynthia M. Katzan, (216) 433-8190.

12a. DISTRIBUTION/AVAILABILITY STATEMENT
Unclassified - Unlimited
Subject Category 91

12b. DISTRIBUTION CODE

13. ABSTRACT (*Maximum 200 words*)

The lunar surface is covered by a thick blanket of fine dust. This dust may be readily suspended from the surface and transported by a variety of mechanisms. As a consequence, lunar dust can accumulate on sensitive power components, such as photovoltaic arrays and radiator surfaces, reducing their performance. In addition to natural mechanisms, human activities on the Moon will disturb significant amounts of lunar dust. Of all the mechanisms identified, the most serious is rocket launch and landing. The return of components from the Surveyor III provided a rare opportunity to observe the effects of the nearby landing of the Apollo 12 lunar module. The evidence proved that significant dust accumulation occurred on the Surveyor at a distance of 155 m. From available information on particle suspension and transport mechanisms, a series of models was developed to predict dust accumulation as a function of distance from the lunar module. The accumulation distribution was extrapolated to a future lunar lander scenario. These models indicate that accumulation is expected to be substantial even as far as 2 km from the landing site. Estimates of the performance penalties associated with lunar dust coverage on radiators and photovoltaic arrays are presented. Because of the lunar dust adhesive and cohesive properties, the most practical dust defensive strategy appears to be the protection of sensitive components from the arrival of lunar dust by location, orientation, or barriers.

14. SUBJECT TERMS	15. NUMBER OF PAGES
Lunar soil; Lunar dust; Particles; Lunar bases; Photovoltaic cells; Radiators; Surveyor III lunar probe	44
	16. PRICE CODE A03

17. SECURITY CLASSIFICATION OF REPORT	18. SECURITY CLASSIFICATION OF THIS PAGE	19. SECURITY CLASSIFICATION OF ABSTRACT	20. LIMITATION OF ABSTRACT
Unclassified	Unclassified	Unclassified	

NSN 7540-01-280-5500

Standard Form 298 (Rev. 2-89)
Prescribed by ANSI Std. Z39-18
298-102

NASA-Langley, 1991